Received: 3 December 2019 | Accepted: 23 April 2020

DOI: 10.1002/hyp.13791

WILEY

A TRIBUTE TO EDWARD P. GLENN (1947-2017): A LEGACY OF SCIENTIFIC ENVIRONMENTAL ASSESSMENT AND APPLICATIONS IN HYDROLOGICAL PROCESSES

Evaluation of WaPOR V2 evapotranspiration products across Africa

Megan L. Blatchford[1] | Chris M. Mannaerts[1] | Sammy M. Njuki[1] | Hamideh Nouri[2] | Yijian Zeng[1] | Henk Pelgrum[3] | Steven Wonink[3] | Poolad Karimi[4]

[1]Faculty of Geo-Information and Earth Observation (ITC), University of Twente, Enschede, The Netherlands

[2]Division of Agronomy, University of Göttingen, Göttingen, Germany

[3]Research and Development, eLEAF BV, Wageningen, The Netherlands

[4]Water Science and Engineering, IHE Delft Institute for Water Education, Delft, The Netherlands

Correspondence
Megan L. Blatchford, Faculty of Geo-Information and Earth Observation (ITC), University of Twente, Hengelosestraat 99, 7514 AE, Enschede, The Netherlands.
Email: m.l.blatchford@utwente.nl

Funding information
UN-FAO; U.S. Geological Survey, Grant/Award Number: MOD16

Abstract

The Food and Agricultural Organization of the United Nations (FAO) portal to monitor water productivity through open-access of remotely sensed derived data (WaPOR) offers continuous actual evapotranspiration and interception (ETIa-WPR) data at a 10-day basis across Africa and the Middle East from 2009 onwards at three spatial resolutions. The continental level (250 m) covers Africa and the Middle East (L1). The national level (100 m) covers 21 countries and 4 river basins (L2). The third level (30 m) covers eight irrigation areas (L3). To quantify the uncertainty of WaPOR version 2 (V2.0) ETIa-WPR in Africa, we used a number of validation methods. We checked the physical consistency against water availability and the long-term water balance and then verify the continental spatial and temporal trends for the major climates in Africa. We directly validated ETIa-WPR against in situ data of 14 eddy covariance stations (EC). Finally, we checked the level consistency between the different spatial resolutions. Our findings indicate that ETIa-WPR is performing well, but with some noticeable overestimation. The ETIa-WPR is showing expected spatial and temporal consistency with respect to climate classes. ETIa-WPR shows mixed results at point scale as compared to EC flux towers with an overall correlation of 0.71, and a root mean square error of 1.2 mm/day. The level consistency is very high between L1 and L2. However, the consistency between L1 and L3 varies significantly between irrigation areas. In rainfed areas, the ETIa-WPR is overestimating at low ETIa-WPR and underestimating when ETIa is high. In irrigated areas, ETIa-WPR values appear to be consistently overestimating ETa. The relative soil moisture content (SMC), the input of quality layers and local advection effects were some of the identified causes. The quality assessment of ETIa-WPR product is enhanced by

combining multiple evaluation methods. Based on the results, the ETIa-WPR dataset is of enough quality to contribute to the understanding and monitoring of local and continental water processes and water management.

KEYWORDS

accuracy assessment, actual evapotranspiration, consistency, continental Africa, direct validation, penman–Montieth, remote sensing, water resources management

1 | INTRODUCTION

Actual evapotranspiration (ETa) is the second largest process in the terrestrial water budget after precipitation (PCP). ETa is also an essential component of plant growth and, therefore, the carbon cycle. Available water resources are becoming, or are already scarce, in many basins worldwide (Degefu et al., 2018). The acceleration of the water cycle from a climate change perspective will further influence water availability not only for human consumption but also our food sources (Rockström, Falkenmark, Lannerstad, & Karlberg, 2012). For this purpose, accurate estimates of ETa are required for several management tasks, including, but not limited to, water accounting, water footprint, basin-wide water balances, irrigation, crop management and monitoring of climate change and its impact on crop production. These activities require ETa at varying extents and spatio-temporal resolutions.

Remote sensing from satellites is perhaps the only feasible means for quantifying and monitoring ETa for wide-areas (Glenn, Huete, Nagler, Hirschboeck, & Brown, 2007). Several remote sensing approaches exist to estimate ETa which include, surface energy balance methods (e.g. Allen, Tasumi, & Trezza, 2007; Bastiaanssen, Menenti, Feddes, & Holtslag, 1998; Su, 2002), Penman–Monteith methods (FAO, 2020a) and more empirical vegetation indices based methods (Glenn, Huete, Nagler, & Nelson, 2008; Nagler, Glenn, Nguyen, Scott, & Doody, 2013). Currently, there are a number of open-access remote sensing-based ETa products based on remote sensing data at the continental and global scale. Global products include: the moderate resolution imaging spectroradiometer (MODIS) based ETa (MOD16) product (Mu, Zhao, & Running, 2011), generated every 8-days at 250 m; the Global Land Evaporation Amsterdam Model (GLEAM) ETa (Miralles et al., 2011), generated daily at 0.25°; the operational Simplified Surface Energy Balance (SSEBop) ETa (Senay, Budde, & Verdin, 2011), generated monthly at 1 km; and the Land Surface Analysis-Satellite Applications Facility (LSA-SAF) Meteostat Second Generation (MSG) ETa (Ghilain, Arboleda, & Gellens-Meulenberghs, 2011), generated daily at approximately 3 km.

Validation of these remote sensing products is an essential step in understanding their applicability and characterize uncertainty. This uncertainty can guide if the ETa product is suitable as input into different water management activities along with the associated risk when making a decision based on the product. Many studies exist that attempt to validate large remote sensing-based ETa datasets. Most studies are focused on one or two validation methods at one scale. The most common validation methods are either point or pixel scale against ground-truth data, like eddy covariance (EC) measurements (e.g. Mu et al., 2011), or spatial intercomparison of a product over regions, land classes, biomes (e.g. Mueller et al., 2011). Some authors validate multiple products against each other for spatial and temporal patterns and against ground-truth data (e.g. Hu, Jia, & Menenti, 2015; Nouri et al., 2016). Liu et al. (2016) evaluated basin-scale ETa estimates against the water balance method. Velpuri, Senay, Singh, Bohms, and Verdin (2013) compared MOD16 (1 km) at point scale to EC and at basin scale to the water balance. Other than a few occasions, for example, Velpuri et al. (2013), these validation efforts often failed to evaluate the product at multi-scale, from pixel to basin or region.

The best-practice validation strategies of big remote sensing datasets have been proposed by Zeng et al. (2015, 2019). They recommend multi-stage validation activities that include combinations of direct validation, physical validation and cross-comparisons. In practice, many developers of remote sensing products include all or at least a combination of these activities during their validation. To name a few, these include the MODIS MODLAND product (Morisette, Privette, & Justice, 2002; Morisette, Privette, Justice, & Running, 1998); Copernicus Global Land Service products Dry Matter Productivity (Swinnen, Van Hoolst, & Toté, 2015); and ASTER land surface temperature (Schneider, Ghent, Prata, Corlett, & Remedios, 2012).

In regions such as Africa, where little observational data is available, validation should utilize all available avenues for ascertaining product quality, with a multi-step and -phase validation strategy that includes direct validation (with ground measurements), physical consistency check and cross-comparisons. As such, the limitations due to the sparseness of available data are reduced, and the product quality is understood from a multi-scale perspective, by using validation best-practice and combining multiple validation techniques.

The latest available database of continental products, released in 2019, for Africa and the Middle East, is now available on FAO portal to monitor water productivity through open-access of remotely sensed derived data (WaPOR; https://wapor.apps.fao.org/home/WAPOR_2/2). It provides the highest available spatial resolution for an operational open-access ETa and interception (ETIa-WPR) product at the continental scale. This article presents a multi-scale validation of the version 2 (V2.0) ETIa-WPR. The results from each validation procedure were analysed individually and then as a whole to determine trends and draw conclusions of the product quality.

2 | DATA AND METHODS

2.1 | The dataset

The analysis dataset is the ETIa-WPR V2.0 products available on the WaPOR portal (https://wapor.apps.fao.org/home/WAPOR_2/1). The ETIa-WPR is based on a modified version of the ETLook model (ETLook-WaPOR) described in Bastiaanssen, Cheema, Immerzeel, Miltenburg, and Pelgrum (2012). The ETLook-WaPOR model uses Penman–Monteith to estimate ETa adapted to remote sensing input data (FAO, 2020a). The Penman–Monteith approach uses the combined approaches of the energy balance equation and the aerodynamic equation and is described in the FAO-56 drainage paper (Allen, Pereira, Raes, & Smith, 1998). The ETIa-WPR defines soil evaporation and transpiration separately using Equations (1) and (2). The interception is a function of the vegetation cover, leaf area index (LAI) and PCP. The ETI-WaPOR is then calculated as the sum of evaporation, transpiration and interception.

$$\lambda E = \frac{\delta(\mathrm{Rn,soil} - \mathrm{G}) + \frac{\rho_{\mathrm{air}}\, C_P(\mathrm{e_{sat}} - \mathrm{e}_a)}{\mathrm{r}_{a,\mathrm{soil}}}}{\delta + \gamma\left(1 + \frac{\mathrm{r}_{s,\mathrm{soil}}}{\mathrm{r}_{a,\mathrm{soil}}}\right)}, \quad (1)$$

$$\lambda T = \frac{\delta(\mathrm{Rn,canopy}) + \frac{\rho_{\mathrm{air}}\, C_P(\mathrm{e_{sat}} - \mathrm{e}_a)}{\mathrm{r}_{a,\mathrm{canopy}}}}{\delta + \gamma\left(1 + \frac{\mathrm{r}_{s,\mathrm{canopy}}}{\mathrm{r}_{a,\mathrm{canopy}}}\right)}, \quad (2)$$

where E and T (mm/day) are the evaporation and transpiration, respectively and λ is the latent heat of vaporization. R_n (MJ m^{-2} day^{-1}) of the soil ($R_{n,soil}$) and canopy ($R_{n,canopy}$) is the net radiation and G (MJ m^{-2} day^{-1}) is the ground heat flux. ρ_{air} (kg/m^3) is the density of air, C_P (MJ kg^{-1} °C) is the specific heat of air,($e_{sat} - e_a$) (kPa) is the vapour pressure deficit (VPD), r_a (s/m) is the aerodynamic resistance, r_s (s/m) is the soil resistance, or canopy resistance when using the Penman–Monteith-model to estimate evaporation or transpiration, respectively. $\delta = d(e_{sat})/dT$ (kPa/°C) is the slope of the curve relating saturated water vapour pressure to the air temperature, and γ is the psychometric constant (kPa/°C). This approach partitions the ETIa-WPR to evaporation and transpiration using the modified versions of Penman–Monteith, which differentiate the net available radiation and resistance formulas based on the vegetation cover according to the ETLook model (Bastiaanssen et al., 2012). A major difference between ETLook-WaPOR and ETLook is the source of remote sensing data for the soil moisture. In the original ETLook soil moisture is derived from passive microwave, and in the WAPOR approach soil moisture is derived from land surface temperature (LST). The WaPOR database provides ETIa-WPR in three spatial resolutions dependent on the location and extent. The products available specifically for Africa are shown in Table 1 and are available online on the WaPOR portal (https://wapor.apps.fao.org/home/WAPOR_2/1).

Interception (I) is the process where the leaves intercept rainfall. Intercepted rainfall evaporates directly from the leaves and requires energy that is not available for transpiration. Interception (mm/day) is a function of the vegetation cover, LAI and PCP.

$$I = 0.2\, I_{lai}\left(1 - \frac{1}{1 + \frac{c}{0.2\, I_{lai}}}\right). \quad (3)$$

C_{veg} is the vegetation cover and is calculated from the normalized difference vegetation index (NDVI) and I_{lai} is the leaf area index converted from c_{veg}.

Datasets (including intermediate datasets) available for the validation include relative soil moisture content (SMC)—a wetness indicator, NDVI, solar radiation (SR), NDVI quality layer, LST quality layer, PCP and reference evapotranspiration (RET) (Table 2). The producers of the datasets in the WaPOR portal—the FAO's Remote sensing-based database for the monitoring of agricultural water and land productivity in Africa and the Middle East (FRAME) Consortium, led by eLEAF and comprised of The Flemish institute for technological research (VITO),

TABLE 1 Description of the WaPOR V2.0 ETIa-WPR data products, available on the WaPOR portal, used for validation in Africa (FAO, 2020b)

	Spatial resolution (m)	Temporal resolution[a]	Spatial extent (in Africa)	Satellite (spatial resolution|return period)
Level I (L1)	250	Dekadal	Continental Africa	MODIS (250 m|1-day)
Level II (L2)	100	Dekadal	Morocco, Tunisia, Egypt, Ghana, Kenya, Niger, Sudan, Mali, Benin, Ethiopia, Rwanda, Burundi, Mozambique, Uganda	MODIS (250 m|1-day)[b] PROBA-V (100 m|2-day)[b]
Level III (L3)	30	Dekadal	Awash, Ethiopia Koga, Ethiopia Office du Niger, Mali Zankalon, Egypt	Landsat (30 m|16-day)

Abbreviations: MODIS, moderate resolution imaging spectroradiometer; WaPOR, water productivity through open-access of remotely sensed derived data.

[a]Dekadal is approximately 10 days. It splits the month into three parts, where the first and second dekads are 10 days and the third dekad covers the remaining days in the month.

[b]MODIS is resampled to 100 m up to 2013 and PROBA-V is used from March 2014.

TABLE 2 Description of the intermediate and product datasets used for the evaluation of ETIa-WPR (FAO, 2020a)

Dataset	Spatial|Temporal resolution/s	Data product/s[a]	Sensor/s[b]
NDVI	Available for L1, L2 and L3 (per Table 1)	MOD09GQ[c], PROBA-V[d], Landsat 5,7,8[e]	MODIS[c], PROBA-V[d], Landsat[e]
SMC		MOD09GQ[c], PROBA-V[d], Landsat 5,7,8[e]	MODIS[c], PROBA-V[d], Landsat[e]
SR		SRTM (DEM)	MSG
LST quality layer	As for L1; Table 1	MOD11A1, MYD11A1	MODIS
NDVI quality later	As for L1; Table 1	MOD09GQ[c], PROBA-V[d], Landsat 5,7,8[e]	MODIS[c], PROBA-V[d], Landsat[e]
PCP	5 km|daily	CHIRPS v2, CHIRP	TRMM, GPM
RET	25 km|daily	SRTM (DEM)	MSG, MERRA/GEOS-5

Abbreviations: LST, land surface temperature; NDVI, normalized difference vegetation index; PCP, precipitation; RET, reference evapotranspiration; SMC, soil moisture content; SR, solar radiation.

[a]CHIRPS, Climate Hazards Group Infrared Precipitation with Station Data; MOD09GQ, MODIS/Terra Surface Reflectance Daily L2G Global 250 m SIN Grid; MOD11A1, MODIS/Terra Land Surface Temperature/Emissivity Daily L3 Global 1 km SIN Grid; MYD11A1, MODIS/Aqua Land Surface Temperature/Emissivity Daily L3 Global 1 km SIN Grid; SRTM, Shuttle Radar Topography Mission (DEM, Digital Elevation Model—90 m).

[b]GEOS-5, Goddard Earth Observing System; GPM, Global Precipitation Measurement; Landsat, Landsat Satellite 5, 7 and 8; MERRA, Modern-Era Retrospective Analysis For Research And Applications; MODIS, Moderate Resolution Imaging Spectroradiometer; PROBA-V, Project for On-Board Autonomy—Vegetation; MSG, Meteosat Second Generation (used for transmissivity); TRMM, Tropical Rainfall Measuring Mission.

[c]L1 data product and sensor.

[d]L2 data product and sensor.

[e]L3 data product and sensor.

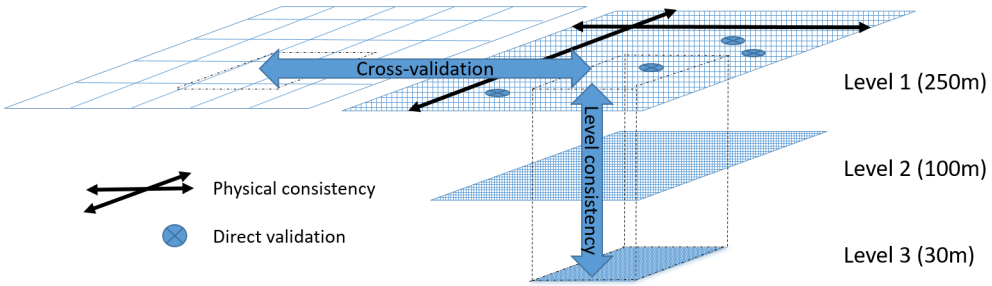

FIGURE 1 Validation approach used in the validation of the ETIa-WPR product in Africa

International Institute for Geo-Information Science and Earth Observation at the University of Twente (ITC-UTWENTE) and WaterWatch—provided the SMC and NDVI layers for the validation. All other layers are available on the WaPOR portal. The NDVI quality layer and the LST quality layer are indicators of the quality of the input satellite data. The NDVI quality layer provides the gap, in days, to the nearest valid observation for that variable. The LST quality layer provides the number of the days between the date of the data file and the earlier remote sensing observation on which the data is based.

WaPOR further relies on input from weather data, air temperature, relative humidity wind speed, which are obtained from Modern-Era Retrospective analysis for Research and Applications (MERRA) up to the start of 21 February 2014 and the Goddard Earth Observing System (GEOS-5) after 21 February 2014 (Rienecker et al., 2011). The weather data is resampled using a bilinear interpolation method to the 250 m resolution. The temperature is also resampled based on elevation data.

2.2 | Validation approach and workflow

The validation approach comprises three components, physical validation, direct validation and level consistency (Figure 1). The physical validation and direct validation were undertaken on the L1 product for the period 2009–2018. The physical validation (Section 2.3) includes an assessment of the water balance and water availability (Section 2.3.1) and a spatial and temporal consistency check (Section 2.3.2) for the extent of Africa. The water balance utilizes other existing continental datasets to complete the water balance and is therefore also considered cross-validation. The spatial and temporal consistency checks if spatial and temporal patterns were being captured. The direct validation (Section 2.4) involves a comparison to ETa estimations from EC stations. The level consistency (Section 2.5) checks for the consistency between levels and therefore indicates if the quality of the L1 product is representative of the L2 and L3 products.

2.3 | Physical consistency

2.3.1 | Water balance and water availability

The basin-scale performance of ETIa-WPR is analysed for 22 major hydrological basins of Africa (Lehner & Grill, 2013) through three approaches (Figure 2). First, the ETIa-WPR was compared to the PCP on an annual basis to analyse the water consumed through ETIa to the water available from PCP.

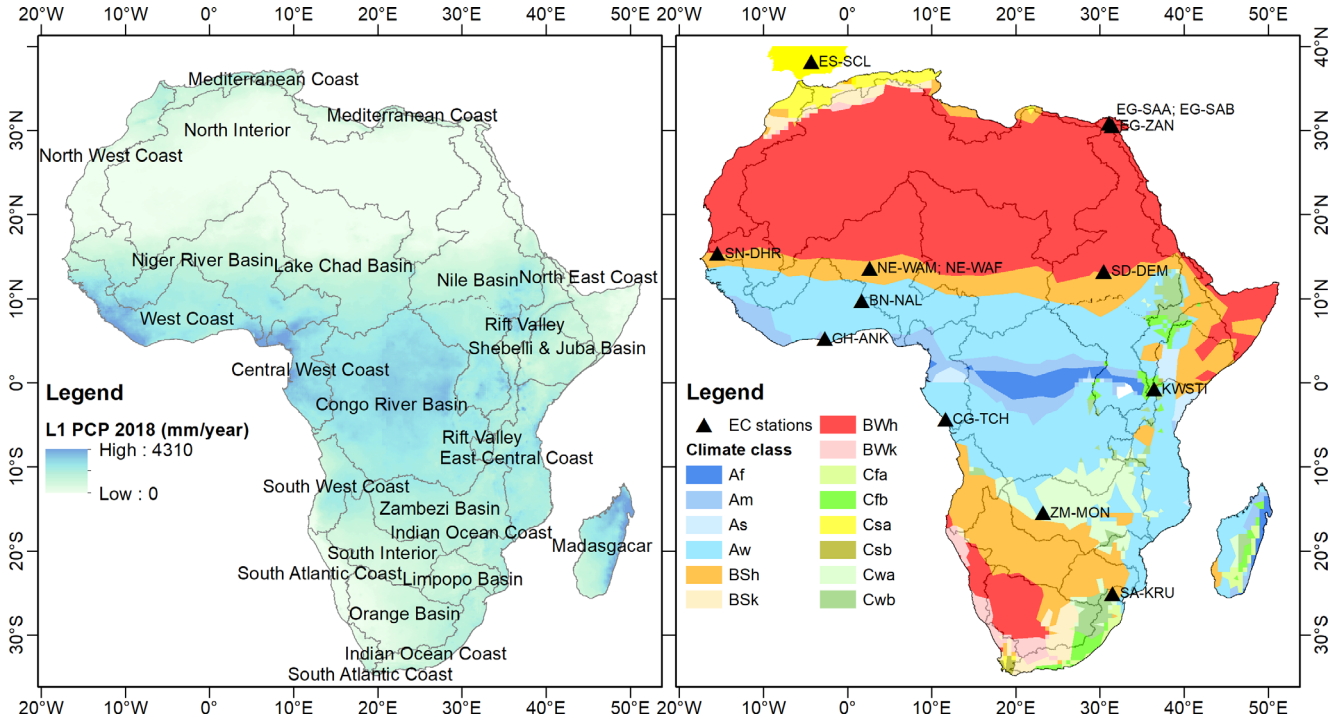

FIGURE 2 Left—A total of 22 major hydrological basins of Africa used in the water balance approach, where the base map is the annual L1 PCP in 2018, available on the WaPOR portal. Right—Koppen–Geiger climate classification and eddy covariance stations where Af, tropical rainforest; Am, tropical monsoon; As, tropical dry savanna; Aw, tropical wet savanna; BSh, arid hot steppe; BSk, arid steppe cold; BWh, arid hot desert; BWk, arid cold steppe; Cfa, temperate without dry season hot summer; Cfb, temperate without dry season warm summer; Csa, temperate dry summer hot summer; Csb, temperate dry summer warm summer; Cwa, temperate dry winter hot summer; Cwb, temperate dry winter–warm summer. Note some stations are in close proximity and are there for represented by one point on the map (e.g. NE-WAM and NE-WAF). PCP, precipitation; WaPOR, water productivity through open-access of remotely sensed derived data

Second, the basin-scale water balance approach compared the long-term ETIa-WPR product to the long-term ETa derived from the water balance (ETa-WB). In many studies, the long-term water balance (>1 year) for large basins assume a negligible change in storage (Hobbins, Ramírez, & Brown, 2001; Wang & Alimohammadi, 2012; Zhang et al., 2012). The long-term water balance, taken from 2009 to 2018 in this case, is therefore defined using Equation (2).

$$\text{ETa-WB}\,(\text{mm/year}) = \text{PCP}\,(\text{m/year}) - \text{Q}\,(\text{mm/year}), \quad (4)$$

where PCP is the long-term precipitation and Q is the long-term basin runoff or streamflow and the ETa-WB is the long-term ETa derived from the water balance. The PCP product found in the WaPOR portal was obtained from the Climate Hazards Group Infrared Precipitation with Stations (CHIRPS) dataset (Funk et al., 2015). The long-term Q was obtained from the Global Streamflow Characteristics Dataset (GSCD) (Beck, De Roo, & Van Dijk, 2015). The GSCD consists of global streamflow maps, including percentile and long-term mean Q at a 0.125° resolution, providing information about runoff behaviour for the entire land surface including ungauged regions.

Third, the ETIa-WPR and PCP annual values were compared to the average ETa from MODIS Global Evapotranspiration Project (ETa-MOD16) for the period 2000–2013 (Mu, Heinsch, Zhao, & Running, 2007; Mu, Zhao, & Running, 2013) and to values from the literature for basins where data is available. The ETa-MOD16 product is also based on the Penman–Monteith equation and considers the surface energy partitioning process and environmental constraints on ETa. The algorithm uses both ground-based meteorological observations and remote sensing observations from MODIS. Basins were not included in the comparison if the ETa-MOD16 data covered less than 80% of the basin area.

2.3.2 | Spatial and temporal consistency

The temporal and spatial trends were observed over the African continent in space and time by observing mean ETIa-WPR, SMC and NDVI for all climate zones during the study period on a dekadal basis. The Koppen–Geiger classification (Figure 2) is used to consider the mean dekadal values for the main climatic zones in Africa (Kottek, Grieser, Beck, Rudolf, & Rubel, 2006). A sample size of 30,000 stratified random pixels is used to represent the continental. This corresponds to less than 0.01% of the total image, however, is considered suitable to represent seasonal trends for the major climate zones. The arid or desert class—B—dominates Africa (57.2%), followed by the tropical class—A (31.0%) and then warm temperate—C (11.8%). The largest sample count corresponds to the largest climatic zones, with a linear 1:1 line representing area to count. The data is further disaggregated

based on the northern and southern hemispheres to account for opposite seasonal patterns.

2.4 | Direct validation

The ETIa-WPR is compared to the in situ ETa from EC fluxes (ETa-EC) at a dekadal scale using 14 locations (13 across Africa and 1 in the Spain extension area) (Figure 2). The country, station code, vegetation, climate zones and available data for comparison—for both WaPOR and the local site, are shown in Table 3. The majority of EC sites are in shrubland or savannas. Egypt stations (EG), the NG-WAM station and GH-ANK station which are located in an irrigated area, agricultural land and forested areas, respectively.

The SA-SKU, SNDHR, GH-ANK, SD-DEM, CG-TCH, ZM-MON and ES-SCL EC sites were obtained from the global Fluxes Database Cluster Dataset (FLUXNET). The FLUXNET 2015 (https://fluxnet.fluxdata.org/) dataset consist of open-source high-quality data products collected from multiple regional networks. The NE-WAM, NE-WAF and BN-NAL sites were obtained from the African Monsoon Multidisciplinary Analysis—Coupling the Tropical Atmosphere and the Hydrological Cycle (AMMA-CATCH) project, aiming at establishing long-term observations on the climate and the environment over Western Africa. KWSTI is operated by the ITC-UTWENTE in partnership with Water Resources Management Authority (WRMA), the Kenya Wildlife Services (KWS) and Egerton University. The EG-ZAN, EG-SAA and EG-SAB sites were operated through the University of Tsukuba, in partnership with Cairo University, National Water Research Center, Delta Barrage, Qalubia, Egypt and the Agriculture Research Center, Giza, Egypt in the Nile Delta. These irrigated sites in the Nile Delta, were under rotation with three major summer crops—rice, maize and cotton—and four major winter crops—wheat, berseem, fava beans and sugar beet.

ETIa-WPR for L1 (250 m) were spatially averaged over a 3×3 pixel window surrounding the EC station, based on the assumption that the window represents the measurement footprint of the EC station. The ETa-EC data was derived from LE flux and then aggregated temporally to dekadal averages to match the temporal resolution of the ETIa-WPR products. Intermediate products, including WaPOR NDVI, SMC and the NDVI and LST quality layers were analysed along with the ETa trends to identify possible sources of error. Reworking the LE flux data to daily values was done [accounting for NaN, non-removed spikes, early morning (dawn) and evening (day-night inversions), dew spiking, etc.] which are not necessarily removed by the standard Eddy Covariance pre-processing software's (converting very high frequency sonic 30-s and gas analyser measurements to 30-min interval fluxes).

The EC method, as a validation method for remote sensing, contains its own inherent errors of up to 10–30%. This uncertainty is related to a number of causes included scale mismatch (where the area of the footprint compared to the remote sensing area compared only partially overlaps), canopy heterogeneities, and measurement problems (Allen, Pereira, Howell, & Jensen, 2011). However, it is fairly common for authors to use EC in heterogeneous landscapes in both validating and driving large remote sensing-based studies (e.g. ETa—Mu et al., 2011; ETa—Velpuri et al., 2013; Sjöström et al. 2013).

The ETIa-EC was also compared against in situ VPD (VPD-EC) and RET (RET-EC). In WaPOR, the VPD and RET are estimated using

TABLE 3 EC site data and descriptions

Site	Country	Ecosystem	Climate	Data-years used	References
SA-SKU	South Africa	Savannas wooded grassland	BSh	2009; 2011	Majozi et al. (2017a)
SN-DHR	Senegal	Savannas	BWh	2010–2013	Tagesson et al. (2015)
SD-DEM	Sudan	Savannas	BWh	2009	Ardö, Mölder, El-Tahir, and Elkhidir (2008)
NE-WAM	Niger	Crops (millet, bare soil, tiger bush)	BSh	2009–2012	Boulain, Cappelaere, Séguis, Favreau, and Gignoux (2009); Ramier et al. (2009)
NE-WAF	Niger	Crops (fallow; shrubs)	BSh	2010–2011	
ES-SCL	Spain	Pasture and Scatter oak trees	Csa	2016–2017	Maria P. Gonzalez (personal communication)
GH-ANK	Ghana	Evergreen broadleaf forests	Am	2011–2014	Chiti, Certini, Grieco, and Valentini (2010)
BN-NAL	Benin	Guinean savanna vegetation	Aw	2009	Mamadou et al. (2014)
KWSTI	Kenya	Open shrubland	Cfb	2012–2014	Odongo et al. (2016)
CG-TCH	Republic of Congo	Savanna grassland	Aw	2009	Merbold et al. (2009)
ZM-MON	Zambia	Savanna woodland	Cwa	2009	
EG-ZAN	Egypt	Irrigated agriculture	BWh	2011–2013	Sugita, Matsuno, El-Kilani, Abdel-Fattah, and Mahmoud (2017)
EG-SAA	Egypt	Irrigated agriculture	BWh	2011–2013	
EG-SAB	Egypt	Irrigated agriculture	BWh	2011–2013	

Abbreviation: EC, eddy covariance.

GEOS-5 (VPD and RET) and MSG (RET only), as compared to being derived from satellite images. GEOS-5 and MSG are available daily and satellite image gaps do not influence the quality of the VPD and RET quality. The RET-EC was estimated using the same method adopted by WaPOR (FAO, 2020a), which is based on FAO-56 (Allen et al., 1998), and was derived from in situ (EC) meteorological data.

$$RET-EC=\frac{\delta(\mathrm{Rn}-\mathrm{G})+\frac{\rho_{air}\,C_p(e_{sat}-e_a)}{r_a}}{\delta+\gamma\left(1+0.34\cdot\frac{r_s}{r_a}\right)}, \quad (5)$$

where r_s is taken as 70 s/m, r_a is taken as $208/u_{obs}$ and u_{obs} is the observed wind speed (m/s) at 10 m.

2.5 | Level consistency

L3 and L2 ETIa-WPR were compared to the L1 data for the period of 2009–2018 on a dekadal basis. A bilinear resampling method was used to spatially aggregate the high-resolution L3 and L2 layers to the resolution of the coarse L1 layer. A random stratified sample of 30,000 points over the entire L2 extent is used for the comparison of the L1 and L2. The L1 and L3 were compared over the entire L3 extent of the Awash, Zankalon, Office du Niger (ODN) and Koga L3 irrigation areas for all pixels. Table 4 shows the description of each L3 irrigated area. The EC station at Zankalon is located in a L3 area. Therefore, as part of the level consistency, all three levels were also compared to the ETa-EC at this station. The method described in Section 2.4 was used to extract the L3 and L3 ETIa-WPR at the station.

3 | RESULTS

3.1 | Physical consistency

3.1.1 | Water balance and water availability

The annual ETIa-WPR divided by the annual PCP (ETIa/PCP) during 2009–2018 for Africa is shown in Figure 3. The annual ETIa-WPR exceeds the annual PCP (ETIa/PCP >1) on 55% occasions for all basins over 10 years study period. The highest number of exceedances occur in 2014 and 2016 (64%), and the lowest number of exceedances occur in 2018 (27%). The majority of these exceedances, 66%, are by less than 10%. The average ETIa-WPR to PCP ratio for the continent of Africa is 0.93. The lowest ratio is in 2010, 0.87, and the highest is in 2015, 0.97. These ratios are significantly higher than the suggested average, 0.65, of ETa to PCP ratio over the global terrestrial surfaces (McDonald, 1961). This ratio is expected to be lower in dry regions or parts of the continent. Except for Lake Chad Basin, basins in the Central, North and West of Africa have ETIa-WPR less than PCP. Most of the exceedances (ETIa > PCP) occur in the South of Africa and on the Horn of Africa.

The basins have the highest ETIa-WPR/PCP ratio in 2015, particularly in Southern Africa. All basins south of Zambezi Basin show a significant decrease in PCP from 2014 to 2015, including a 246, 98 and 238 mm/year drop in Limpopo, Orange and the South Interior respectively. In the same timeframe, the largest ETIa-WPR change is in Limpopo, with a 17 mm/year increase, followed by the South Atlantic Coast with a 35 mm/year decrease. The decrease in PCP is attributed to the drought in this region during this period as a result of the El Nino climatic event (USAID, 2016). However, ETIa-WPR does not seem to respond appropriately to these extreme drops in PCP, which is likely because the SMC does not show any significant response to reduced PCP in this period. The PCP drop in 2015 in drought affected basins ranged from 16.8 to 39.1% of the 2009–2018 average while the SMC drop only ranged from 2.2 to 6.0%. Therefore, the ETIa-WPR is not being properly limited by reduced water availability in the soil.

The average (av.), minimum (min) and maximum (max) annual ETIa-WPR and PCP values for the 2009–2018 period are shown in Table 5. Where literature values were available, annual estimates of ETIa-WPR and PCP are compared with historical estimates on annual ETa and PCP, with ETa from MODIS Global Evapotranspiration Project (ETa-MOD16) and with the ETa-WB. In most cases, the ETIa-WPR is larger than the ETa values in literature, from the water balance and from MOD16. The PCP falls within the range of literature for all but three basins. The PCP is less than that found in literature in the Limpopo and Orange Basin, which is also likely due to the drought in this region which occurred after the estimates as reported in the literature. It is also important to note that the Congo River Basin, Central West Coast and west coast basins have vast areas of low-quality NDVI and LST layers for much of the year. They are making the

TABLE 4 Description of L3 irrigated scheme areas used in the product evaluation

	Awash	Koga	Zankalon	Office du Niger
Average plot size of irrigated area (ha)	10.40	0.24	0.21	5.93
SD plot area (ha)	6.24	0.12	0.13	0.46
Major crops in the irrigated area	Major: sugarcane. Minor: haricot, crotalaria	Wheat, rice, maize, cotton, sugar beet, berseem, fava bean, tomato, potato	Wheat, maize, potato, onion, cabbage, barley	Rice, sugarcane
Vegetation in the non-irrigated area	Savannah	NA	Rainfed agriculture: maize, millet, teff, barley	NA

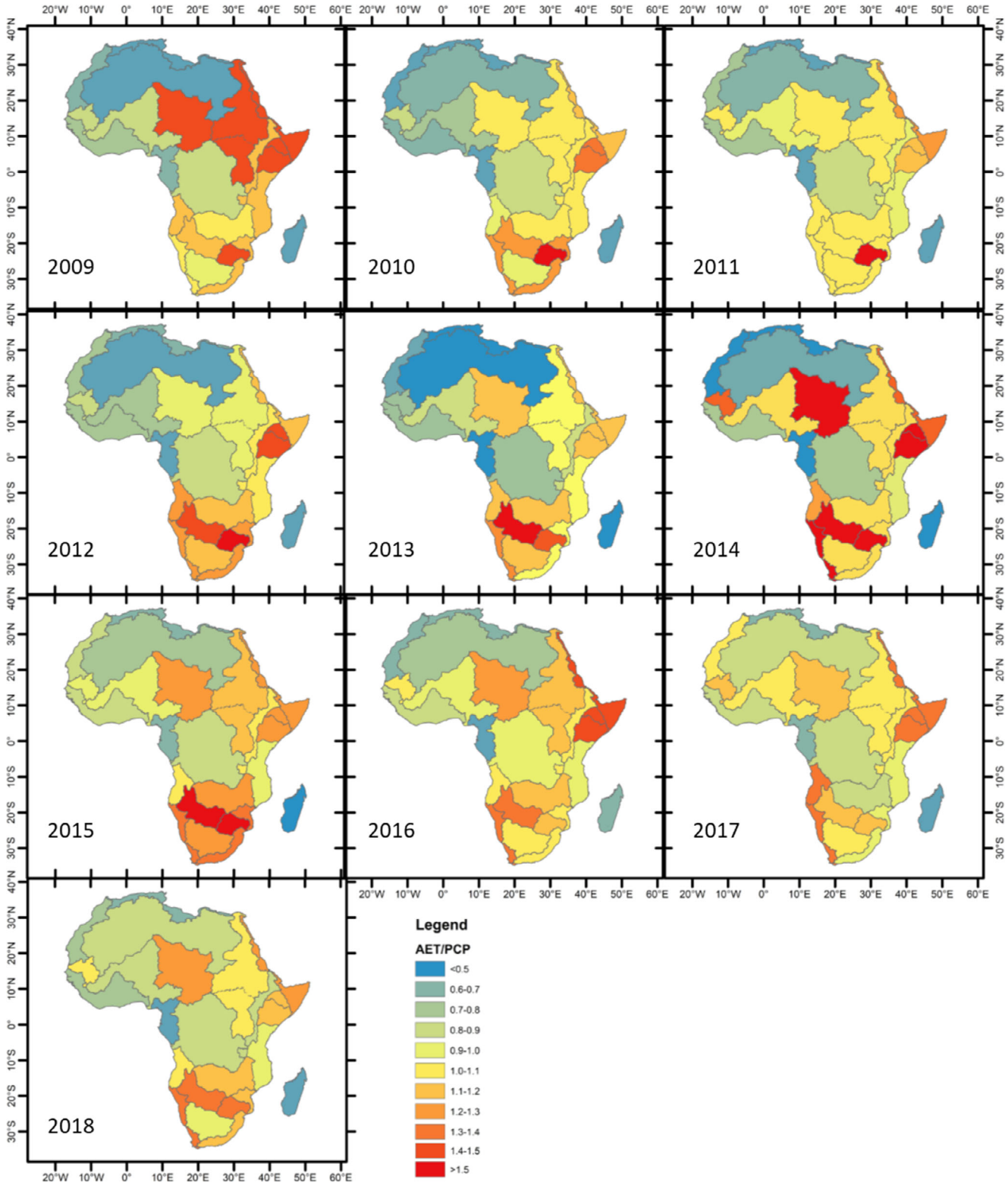

FIGURE 3 Annual ETIa-WPR/PCP in L1 for the 22 major hydro-basins in Africa for the period 2009–2018. PCP, precipitation

annual mean ETIa-WPR values derived from remote sensing much less reliable in these basins.

The ETIa-WPR and ETa-MOD16 are plotted against the ETa-WB in Figure 4. The relationship between both the ETIa-WPR and ETa-MOD16 products show strong linear relationships with ETa-WB. While the ETa-WPR product has a better R^2, the ETa-MOD16 has a lower bias. The ETIa-WPR shows a slightly positive bias, which is increasing with increasing ETa-WB. The absolute difference between

TABLE 5 The annual PCP and ETIa (min and max) of major basins derived from the WaPOR database for the period 2009–2018 compared against the available values in literature and the ETa-WB (all values are mm/year)

Basin	PCP_{WaPOR} av. (min|max)	PCP literature	ETIa-WPR av. (min|max)[a]	ETa-MOD16[a]	ETa literature	ETa-WB
Lake Chad Basin	374 (322|442)	236–451[1–3]	437 (399|471)	–	216–363[1,3]	346
Nile Basin	649 (538|706)	512–693[1,2,4]	714 (685|737)	–	416–515[1,4]	–
Senegal River Basin	548 (472|630)	252–550[1,2]	529 (475|589)	–	258–323[1]	468
Rift Valley	762 (682|887)	650[2]	771 (727|803)	568	–	591
Niger River Basin	679 (625|754)	423–740[1–3]	618 (583|665)	–	329–410[1,3]	553
Shebelli and Juba Basin	474 (400|602)	435–518[2,5]	615 (559|698)	455	504	367
Central West Coast	1847 (1,598|1,908)	1,785[2]	1,108 (1,046 |1,177)	1,159	–	959
Congo River Basin	1,517 (1,452 |1,600)	1,165–1,689[1,2]	1,318 (1,253 |1,401)	949	1,004–1,098[1,6]	–
East Central Coast	966 (876|1,135)	960[2]	970 (928|1,038)	872	–	784
South West Coast	861 (697|984)	940[2]	968 (886|1,078)	758	–	676
Zambezi Basin	928 (772|1,094)	732–1,016[1,2,7]	1,006 (942|1,069)	627	637–798[1,7]	–
Limpopo Basin	519 (326|683)	530–648[1,8]	770 (662|845)	396	516–569[1]	474
Orange Basin	303 (213|368)	325–393[1,2]	320 (272|388)	–	306–335[1]	280

Note: [1]Voisin, Wood, and Lettenmaier (2008); [2]FAO (1997); [3]Li, Coe, and Ramankutty (2005); [4]The Nile Basin Initiative Secretariat (2014); [5]Sebhat and Wenninger (2014); [6]Chishugi and Alemaw (2009); [7]Matondo and Mortensen (1998); [8]LBPTC (2010).
Abbreviations: PCP, precipitation; WaPOR, water productivity through open-access of remotely sensed derived data.
[a]av(min|max) are the yearly average, minimum and maximum for that basin.

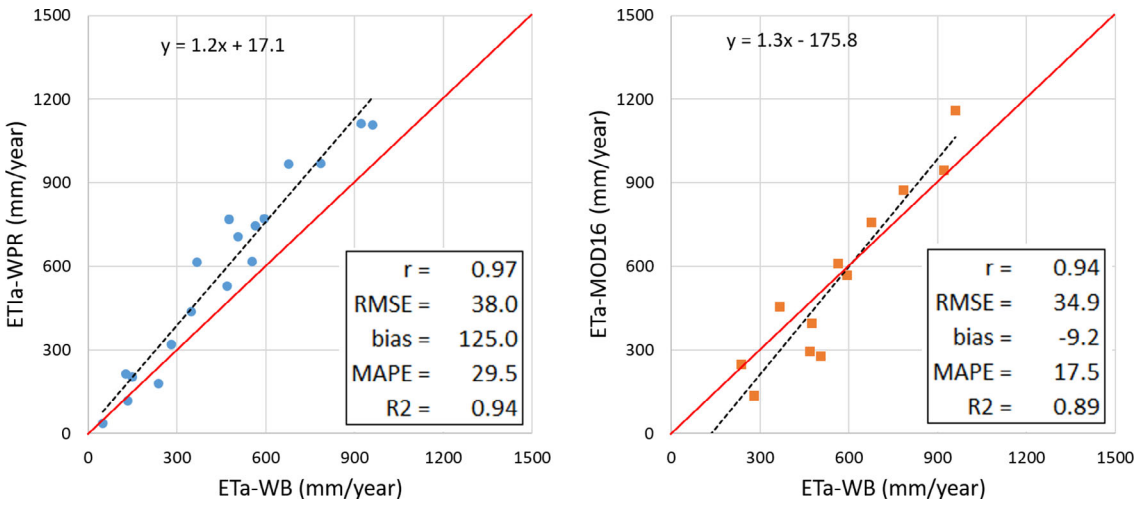

FIGURE 4 The relationship between long-term average annual ETIa-WPR (mm/year) (left) and the ETa-MOD16 (right) plotted against average annual ETa-WB (mm/year) for the 22 major hydrological basins of Africa. The black dotted line is the linear regression and the red line is the 1:1 line

the ETIa-WPR and the ETa-WB is typically increasing with increasing ETa-WB. The relative differences between ETIa-WPR and ETa-WB are lower at high ETa values. The absolute difference and relative difference between ETIa-WPR and ETa-MOD16 were greater at lower ETa-MOD16. The absolute relative difference, between ETIa-WPR and ETa-WB typically decreased with increasing PCP. The long-term ETIa-WPR is larger than the ETa-WB on 13 out of 22 basins. The Q represented from 4.4% (South Interior) up to 47.0% (Central West Coast), with a median of 18.6%, of the long-term PCP. The Q is greater in basins with greater ETIa-WPR and PCP. In basins where the long-term average Q is less than 150 mm/year (18 basins), the relative difference between ETa estimates ranged from −20 to +70%. When the long-term average Q is greater than 200 mm/year the relative difference ranged from −12 to +20%.

The long-term (2009–2018) ETIa-WPR for basins in Africa is estimated to be 590.6 mm/year, which is 12.2% larger than the long-term ETa-WB, estimated to be 518.7 mm/year. The 2010 ETa average for the entire WaPOR extent is compared against ETIa-WPR V1 and other models in Figure 5. These values are sourced from the WaPOR V1 validation report (FAO and IHE Delft, 2019) and include three remote sensing-based surface energy balance models—Atmosphere-Land Exchange Inverse (ALEXI), Surface

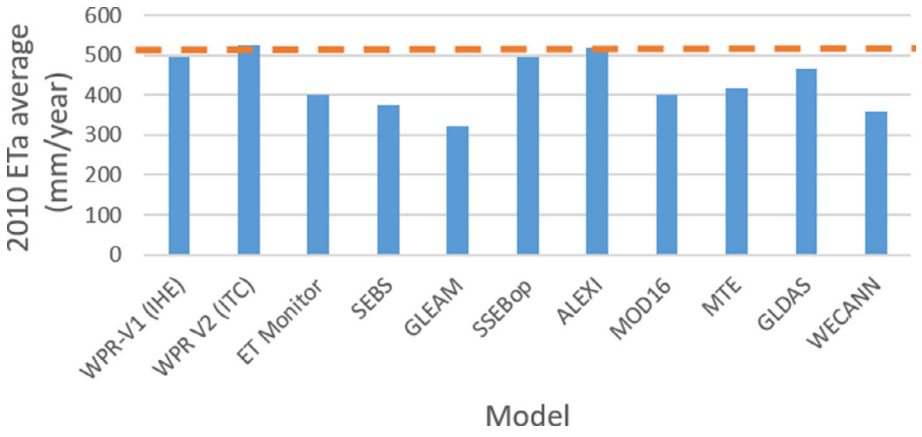

FIGURE 5 2010 continental ETa of various models (values taken from FAO 2019) and ETIa-WPR. The orange dotted line represents the ETIa-WPR and was used for reference to other datasets

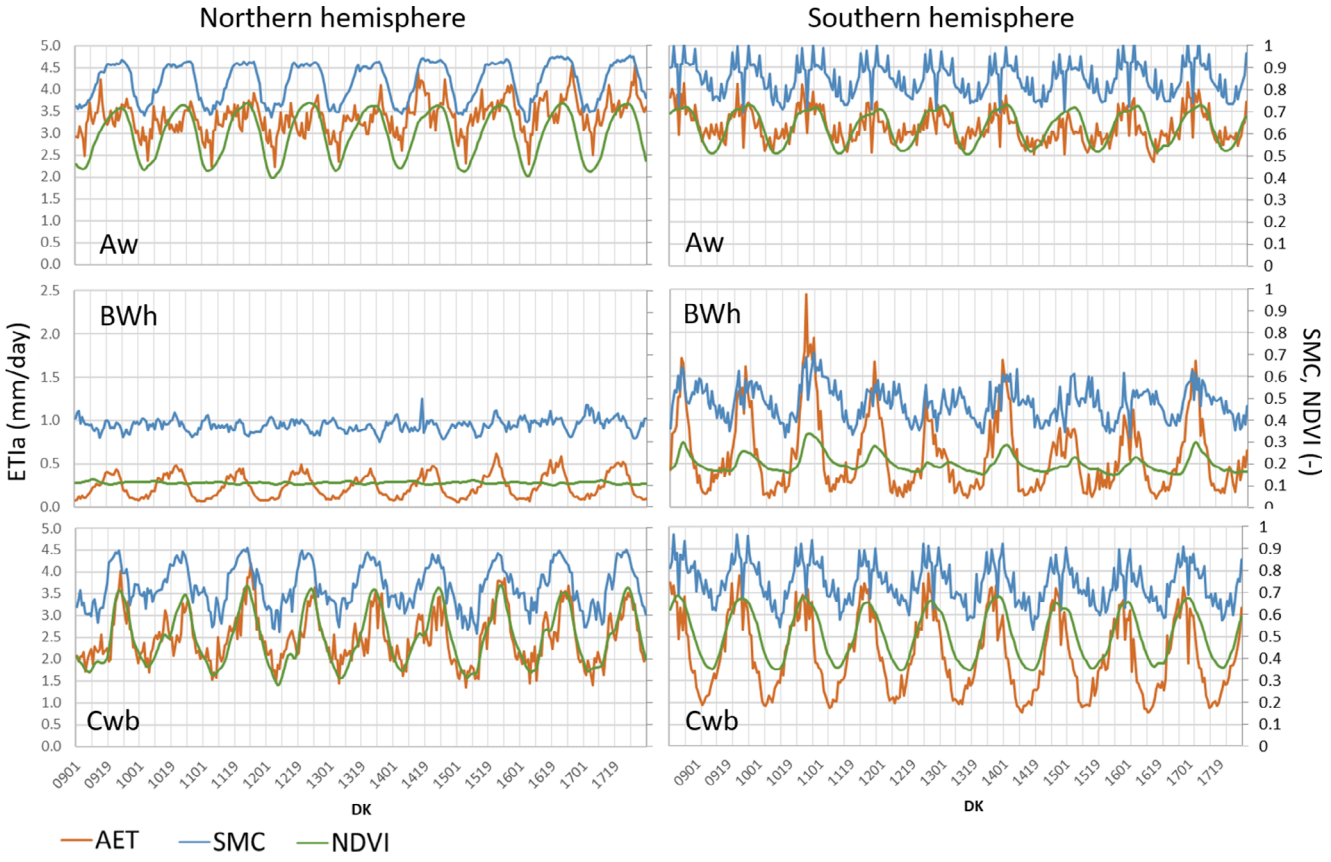

FIGURE 6 Times series of average ETIa-WPR (orange line), SMC (blue line) and NDVI (green line) in tropical wet savanna (Aw), hot arid desert (BWh) and sub-tropical highland climate classes (Cwb) in the northern hemisphere (left) and southern hemisphere (right). Note that BWh has a different ETIa-WPR *y*-axis range to Aw and Cwb. NDVI, normalized difference vegetation index; SMC, soil moisture content

Energy Balance System (SEBS), and SSEBop v4, a remote sensing-based Penman–Monteith approach—MOD16, a remote sensing-based artificial neural network product—Water, Energy, and Carbon with Artificial Neural Networks (WECANN), a hybrid remote sensing-based model—ETMonitor, a land surface models with remote sensing data assimilation—Global Land Data Assimilation System (GLDAS), a Priestley-Taylor approach driven by meteoroidal data—GLEAM v3.2, and, an upscaled FLUXNET product—Multi-Tree Ensemble (MTE). The ALEXI and SSEBop v4, both remote sensing-based surface energy balance models, have a similar performance, 519 and 497 mm/year, respectively. All other approaches, including SEBS, MTE, ETMonitor, WECANN, MOD16, GLEAM v3.2 and GLDAS, report a lower average annual ETa in 2010, ranging from 11% lower (GLDAS) to 38% lower (GLEAM). As compared to the CHIRPS PCP product, ETa as estimated from these products are consuming 54% (GLEAM) to 78% (GLDAS) of the PCP. Compared to

the models with higher ETa that are consuming 83% (SSEBop) to 87% (ALEXI).

3.1.2 | Spatial and temporal consistency

The mean ETIa-WPR, SMC and NDVI were plotted for all climate zones for the northern and southern hemisphere. Figure 6 shows some examples of the largest sub-zones per main climate; wet tropical-savanna (Aw), arid-desert-hot (Bwh) and temperate dry winter–warm summer (Cwb). The average ETIa-WPR (*y*-axis on the left), and SMC and NDVI (*y*-axis on the right) are reported from dekad 0901 (2009—dekad 1) to 1836 (2018—dekad 36).

The temporal trend for each climate zone is inversed between hemispheres, reflecting the opposite seasons between hemispheres. For example, peak ETIa-WPR values occur around dekad 19 and trough values occur around dekad 01 in the northern hemisphere. Conversely, in the southern hemisphere, peak ETIa-WPR values occur around dekad 01 and trough values occur around dekad 19. The inverse pattern highlights the need to separate climate zones based on hemisphere, as these trends would otherwise cancel out and flatten out temporal trends.

The Aw zones are maintaining the highest ETIa-WPR values and shows the lowest relative variability throughout the year. The BWh zones consistently have lower ETIa-WPR values. The BWh in the southern hemisphere is higher than in the northern hemisphere, and the relative intra-annual variation is greater. The ETIa-WPR in these zones follows a clear seasonal pattern, that is not evident from the NDVI or the SMC. The ETIa-WPR is predominantly governed by evaporation in these arid zones, which is indicated by the low NDVI all year round. The temperate zone, Cwb, shows the greatest intra-annual variability in ETIa-WPR, which reflects the more dramatic climatic seasonal variation in these years. ETIa-WPR in Cwb in the northern hemisphere shows two peaks per year. The two seasons are consistent with the zones' location in the Rift Valley of Eastern Africa. The Rift Valley experiences two wet seasons as influenced by the intertropical convergence zone (Hills, 1978). The wet months are March through May and October through December with higher PCP in the March through May period.

ETa is either controlled by available energy or available water. All zones, other than BWh and Aw in the northern hemisphere, show a clear relationship between the ETIa-WPR and the NDVI and SMC. The Aw zone in the northern hemisphere shows two ETIa-WPR peaks a year, however, the SMC and NDVI show one. Despite water being available through SMC in this zone during peak NDVI, there is a drop in ETIa-WPR, suggesting that during this period the ETIa-WPR is limited by solar radiation or available energy. Although not shown here—ETIa-WPR in BWh in the northern hemisphere follows the same seasonal trend as radiation. In the Aw zone in the northern hemisphere, the net radiation peaks several dekads before the NDVI and SMC, resulting in a double-peaked ETIa-WPR. The ETIa-WPR in BWh zone shows a clear seasonal trend, despite no clear seasonal NDVI or SMC trend. Therefore, it is governed by the amount of solar radiation which has a clear yearly trend at the latitudes within the BWh zone.

The SMC appears high in the arid zones, particularly considering such low NDVI in these regions. For example, in BWh in the northern and southern hemisphere, the mean SMC for the climate zone, across all dekads in the study period, never drops below 0.3 and 0.32, respectively. These regions have high potential energy and are typically water constrained. As the SMC is high in these areas with high energy availability, it is resulting in a higher than expected ETIa-WPR in these zones. The SMC, NDVI or ETIa-WPR do not seem to be responding to the drought in the region, where decreasing PCP values should result in reduced SMC and ETIa-WPR during the 2014–2015 period. The low NDVI values indicate that it is the evaporation component (driven by SMC, solar radiation and soil resistance) that is being overestimated in these dry regions.

3.2 | Direct validation

The agreement between ETIa-WPR and ETa-EC is shown in Figure 7 and Table 6. Figure 7 shows the time series of ETIa-WPR and ETa-EC for all available in situ data from all EC stations. Table 6 shows the corresponding metrics for each station, including correlation (*r*), root mean square error (RMSE), bias, mean average percent error (MAPE) the coefficient of determination (R^2) and the average NDVI and LST quality for the comparison period. A good overall correlation ($r = 0.71$) is found between all sites and observations. Substantial variations existed between sites. Consistency in results is seen between years for most sites. The ETIa-WPR typically captured seasonality at most sites.

The best-performing sites in terms of correlation and R^2 are SN-DHR, SD-DEM, EG-ZAN, EG-SAA and EG-SAB. These sites are characterized by arid or semi-arid climates and short vegetation. SN-DHR and EG-SAB also have the best performance in terms of MAPE. The ETIa-WPR closely follows the ETa-EC at the SN-DHR and SD-DEM site, and both respond quickly to rainfall events. At each of these sites the WaPOR SMC and NDVI are well related to both the ETa-EC and ETIa-WPR. For example, the R^2 for the SMC or NDVI and ETa-EC or ETIa-WPR ranges between 0.82–0.87 at SN-DHR and 0.69–0.86 at SD-DEM. SD-DEM does overestimate ETIa-WPR when ETa-EC is low and NDVI is low. These sites are also associated with having high-quality LST and NDVI layers (the average LST quality for the comparison period is equal to or less than 1).

The next best-performing sites, in terms of correlation and R^2, are ES-SCL, ZM-MON and CG-TCH. Excluding CG-TCH, these sites also have good quality NDVI and LST quality layers. The reasonable performance at the CG-TCH station is because the variation in ETa-EC and ETIa-WPR is well related to the VPD derived from the EC station and RET, with $R^2 = 0.62$ and 0.66, respectively. The VPD and RET are derived from GEOS-5 (VPD and RET) and MSG (RET only), as compared to being derived from satellite images. GEOS-5 and MSG are available daily and satellite image gaps do not influence the quality of the VPD and RET quality.

The irrigated agriculture sites, EG-ZAN and EG-SAB, despite high correlation and R^2, are systematically larger than the ETa-EC during

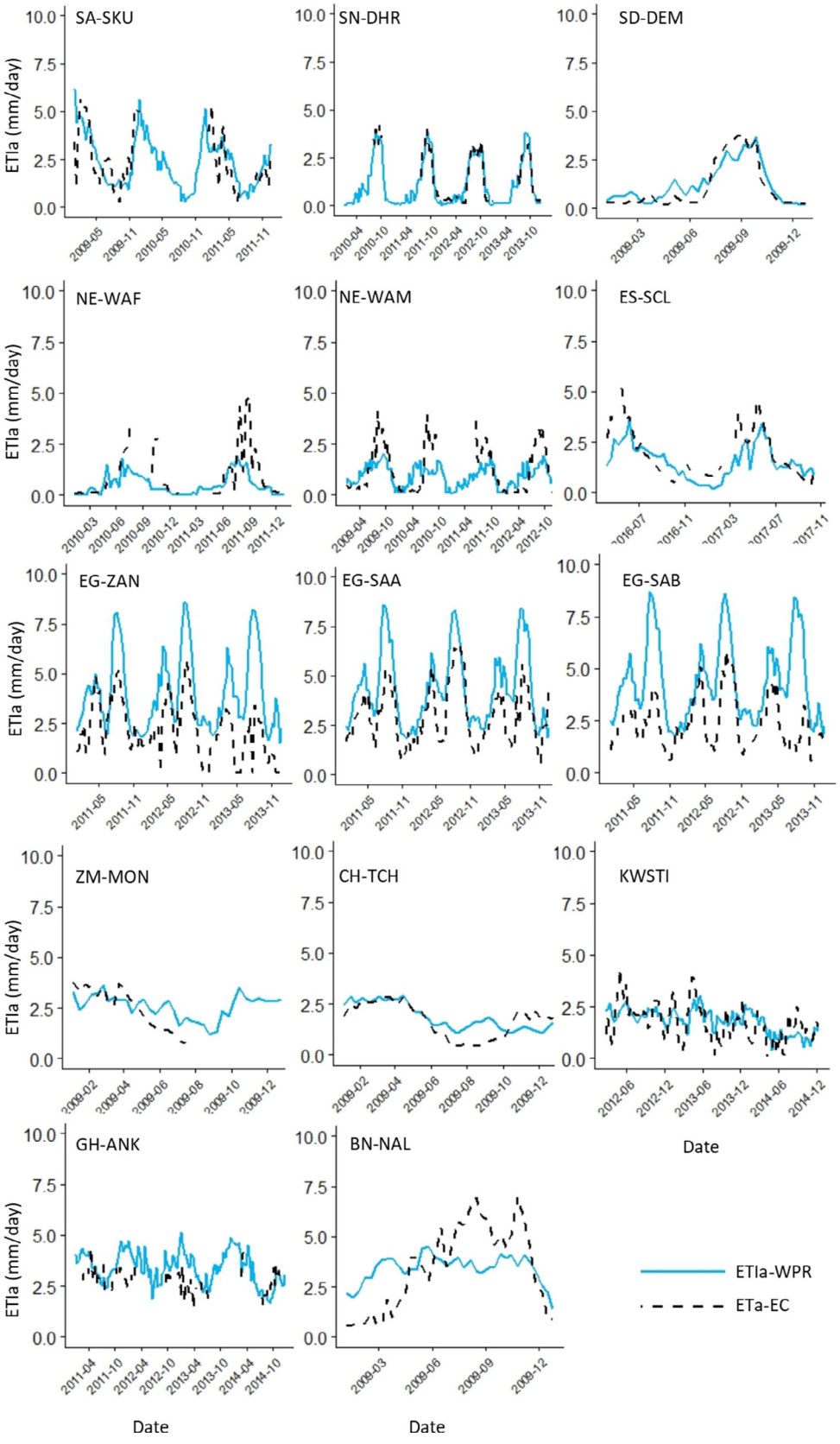

FIGURE 7 Time series of dekad ETIa-WPR (mm/day) (solid blue line) and dekad ETa-EC (mm/day) (dashed black line) for the available periods which varies for different sites. Note that the dates are reported in YYYY-MM format

both high and low ETa-EC, as indicated by the average daily bias (Table 6). This was less evident at EG-SAA. The seasonal values ETIa-WPR and ETa-EC for the summer maize 2012 crop at EG-ZAN are 682 and 424 mm, respectively. Compared to ETa from a lysimeter (ETa-lys), 543 mm, as cited in literature (Atta, Gaafar, Hassan, & El, 2015), at EG-ZAN for the same crop and period. It, therefore,

TABLE 6 Statistics comparing dekadal ETIa-WPR with ETa-EC in 14 locations; more information about sites is available in Table 3

	Dekad count	RMSE (mm/day)	Bias (mm/day)	MAPE (%)	R^2	r ETa-EC	r VPD-EC	r RET-EC	NDVI QUAL[a]	LST QUAL[a]
SA-SKU	63	1.1	0.1	36.3	0.47	0.46	—	—	5.5	0.9
SN-DHR	72	0.4	0.0	17.2	0.92	0.96	−0.43	−0.59	2.0	0.9
SD-DEM	33	0.6	0.3	48.4	0.80	0.90	−0.47	−0.70	1.7	0.5
EG-ZAN	95	2.2	1.7	68.9	0.69	0.68	0.43	0.37	1.3	0.2
EG-SAA	108	0.9	0.8	16.5	0.72	0.75	0.39	0.47	1.4	0.3
EG-SAB	104	1.3	1.6	59.9	0.54	0.58	0.46	0.41	1.3	0.3
NE-WAF	49	1.12	−0.5	67.2	0.31	0.56	−0.45	—	7.4	1.3
NE-WAM	118	0.9	−0.2	58.6	0.40	0.63	—	—	6.3	1.3
ES-SCL	45	0.9	−0.3	34.0	0.52	0.72	−0.47	—	NA	NA
GH-ANK	80	1.0	0.6	28.3	0.12	0.34	0.35	−0.36	99.5	18.0
BN-NAL	36	1.8	0.0	44.9	0.27	0.52	−0.22	−0.82	11.3	2.1
CG-TCH	36	0.6	0.2	27.3	0.55	0.74	0.79	0.95	227.0	23.8
ZM-MON	20	0.8	0.2	27.3	0.48	0.69	−0.59	−0.64	7.0	1.0
KWSTI	98	0.8	0.1	37.7	0.26	0.53	−0.15	—	1.5	0.8
Overall	**957**	**1.2**	**0.5**	**40.4**	**0.54**	**0.71**	**—**	**—**	**—**	**—**

Abbreviations: LST, land surface temperature; MAPE, mean average percent error; NDVI, normalized difference vegetation index; RET, reference evapotranspiration; RMSE, root mean square error; VPD, vapour pressure deficit.

[a]The NDVI quality layer provides the gap, in days, to the nearest valid observation for that variable. The LST quality layer provides the number of the days between the date of the data file and the earlier remote sensing observation on which the data is based.

suggests that the ETa at the irrigated sites fall somewhere between the ETa-EC and L1 ETIa-WPR. The overestimation is likely directly related to the net radiation difference between the EC and WaPOR datasets as inferred from the RET estimated from the EC data and compared to the WaPOR RET. The WaPOR RET has a high linear agreement with the EC RET (R^2 = 0.93). However, the bias of WaPOR RET is consistently 50% greater than the EC RET.

ETIa-WPR and ETa-EC show a weak correlation at NE-WAF and NE-WAM. The ETIa-WPR begins increasing earlier in the season, particularly at NE-WAM, and although the ETIa-WPR is capturing the seasonal trend, it is not capturing the magnitude of the ETa-EC summer values. The difference is likely related to the low-quality NDVI and LST layers during the summer (average annual values LST and NDVI gaps appear low in Table 6, however major gaps are concentrated in the summer season). These sites are not highly correlated with the site VPD or RET and therefore the lower quality LST and NDVI is expected to have a great impact on the quality of ETIa-WPR here. The ETIa-WPR is strongly related to the SMC at these sites (e.g. R^2 = 0.73 at NE-WAM); however, the ETa-EC shows no relationship with the WaPOR SMC (R^2 = 0.37 at NE-WAM). Both of these sites are dominated by evaporation (in WaPOR) for most of the year—as indicated by low NDVI all year.

The ETIa-WPR performance at BN-NAL is not capturing the site seasonality. BN-NAL ETIa-WPR and ETa-EC show annual values ranging from 1.4–4.5 mm/day to 0.6–6.9 mm/day, respectively. The ETIa-WPR at BN-NAL does not appear to capture the rainy period in July–September where the highest gaps in the NDVI exist (low NDVI quality). At this site, the WaPOR SMC and NDVI layers have a stronger relationship with the ETa-EC than the ETIa-WPR. For example, the R^2 between the WaPOR NDVI and the ETa-EC and the WaPOR NDVI and the ETIa-WPR are 0.87 and 0.56, respectively. This is, therefore, pointing to an overestimation of the evaporation component when NDVI is low and an underestimation of the transpiration component when the transpiration is high.

The ETIa-WPR has the lowest performance at the GH-ANK and KWSTI in terms of both the regression and the temporal trends. The GH-ANK site is characterized by a tropical climate and high vegetation height (evergreen forest). Further, the ETa-EC is not strongly related to the VPD or the RET at both GH-ANK and KWSTI. The VPD at this site ranges from 0.07 to 0.81 with high relative humidity. The KWSTI site is located in the Rift Valley, between the Aberdares Ranges to the east and the Mau escarpment to the west. This setting creates a complex microclimate with significant diurnal variation in temperature and wind speed, among other meteorological variables. This site has an inferior NDVI quality layer and a very low correlation with VPD. As a result, errors in the input meteorological data may highly influence ETa-EC estimates at the site.

The results show noticeable improvement for all metrics on average across all sites on a monthly scale (Figure 8 and Table 7). The overall correlation improved by 0.1, the overall RMSE reduced by 0.6 mm/day, the bias reduced by 0.2 mm/day, the MAPE reduced by 14.1% and the R^2 increased by 0.06. The correlation improved at each site and the bias decreased at each site except NE-WAM and

ZM-MON. The increase at NE-WAM may be a result of missing EC data during the dry season, creating a bias in favour of the wet season. The RMSE increased at the Egypt sites and at BN-NAL, likely due to the strong bias they displayed at a dekadal scale in both wet and dry seasons in favour of ETIa-WPR which aggregated at a monthly scale. Other sites showed underestimations in the wet season and overestimations in the dry season, flattening out bias over time. The MAPE increased significantly at EG-SAA. EG-SAA followed the temporal profile more closely and showed the least bias compared to EG-ZAN and EG-SAB. Overall, at a monthly scale ETIa-WPR is still overestimating ETa-EC at low ETa and at high ETa the linear regression conforms with the 1:1 line. However, if the Egypt sites are excluded from the analysis, the ETIa-WPR is overestimating ETa-EC when ETa-EC is less than 1.6 mm/day and underestimating ETa-EC when ETa-EC is greater than 1.6 mm/day.

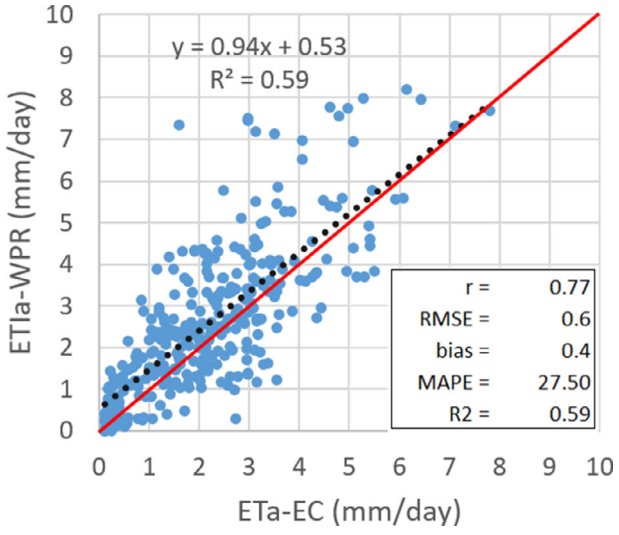

FIGURE 8 The relationship between monthly mean daily ETIa-WPR (mm/day) plotted against monthly mean daily ETa-EC (mm/day). Only months with valid observations for all dekads within that month are included. The dotted black line represents the linear regression, and the red line represents the 1:1 line

3.3 | Level consistency

The consistency between the ETIa data products for the L1 and L2 data products is high. The ETIa-WPR RMSE, between L1 and L2, for each dekad for the 2009–2018 period ranged from 0.0 to 0.1 mm/day, while the correlation ranged from 0.95 to 1.00 with a median of 0.98. The median R^2 over the period is 0.96 while the median bias is 7%. The consistency between layers dropped slightly after 2014, coinciding with the introduction of PROBA-V in March 2014. The median correlation dropped from an approximately perfect positive linear correlation (~1.00) to 0.96, and the median RMSE increase was negligible (<0.1 mm/day). A slight positive systematic bias, in favour of L2, is evident after 2014, with median bias increased from 4 to 9%.

The L1 and L3 ETIa-WPR products have a lower consistency as compared to the L1 and L2 products in the four irrigation areas. The mean ETIa-WPR values for all dekads in the Zankalon and Awash schemes are shown in Figure 9. The Awash area has the highest consistency of all scheme areas, reflected in the highest average correlation and R^2 across dekads, 0.84 and 0.71 respectively. The ETIa-WPR RMSE between L1 and L3 in the Awash ranges from 0.42–1.0 mm/day, while the correlation ranges from 0.63 to 0.92. The median correlation for all dekads in the study period is 0.84, and the median R^2 is 0.84. The RMSE is highest when the ETIa-WPR is highest. The RMSE temporal trend is in line with the seasonal trend in the Awash and displays the two seasons associated with the

TABLE 7 Statistics comparing monthly ETIa-WPR with ETa-EC in 14 locations; more information about sites is available in Table 3

	Month count	RMSE (mm/day)	Bias (mm/day)	MAPE (%)	*r*	R^2
SA-SKU	22	0.9	0.1	30.4	0.76	0.57
SN-DHR	28	0.3	0.0	13.9	0.98	0.95
SD-DEM	11	0.5	0.3	44.8	0.92	0.85
EG-ZAN	33	2.1	1.7	69.5	0.75	0.57
EG-SAA	36	1.4	0.8	31.7	0.77	0.6
EG-SAB	32	1.7	1.3	45.8	0.76	0.58
NE-WAF	19	1.0	−0.5	59.5	0.73	0.53
NE-WAM	41	0.9	−0.3	54.9	0.70	0.49
ES-SCL	19	0.8	−0.3	36.4	0.77	0.6
GH-ANK	34	0.9	0.6	26.9	0.45	0.2
BN-NAL	12	1.7	0.0	42.9	0.58	0.34
CG-TCH	12	0.6	0.2	25.9	0.76	0.58
ZM-MON	6	0.7	0.1	19.8	0.67	0.45
KWSTI	35	0.7	0.1	31.7	0.54	0.3
Overall	340	0.6	0.4	26.3	0.77	0.59

Abbreviations: LST, land surface temperature; MAPE, mean average percent error; NDVI, normalized difference vegetation index; RMSE, root mean square error.

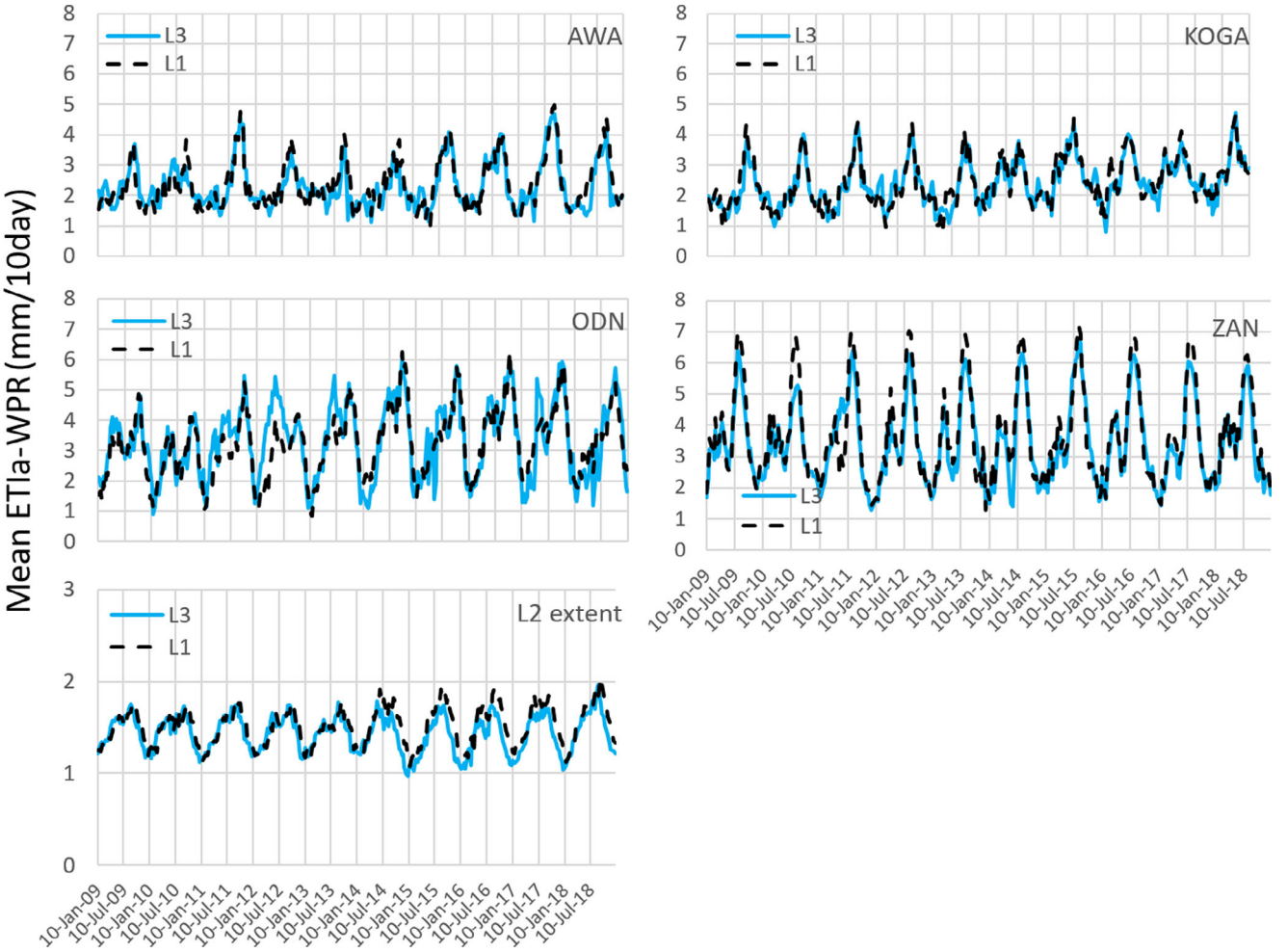

FIGURE 9 Mean ETIa-WPR per dekad (mm/day) in continental level—L1 (blue line) and irrigation scheme level—L3 (black line) for 2009–2018 period in each of the L3 extents (Table 1) and the continental level—L1 (blue line) and basin and country level—L3 (black line) in the L2 extent. Note that the date is reported in YYYY-MM

FIGURE 10 Level consistency validation of ETIa-WPR for three levels of L1, L2 and L3 ETIa-WPR in comparison with ETa-EC per dekad (Dk) for the 2011–2013 period at EG-ZAN EC station

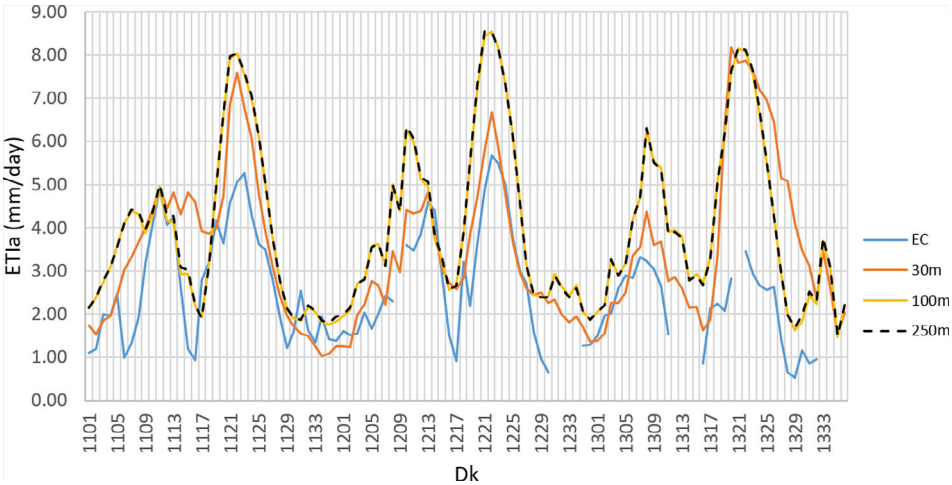

intertropical convergence zone. The correlation is above 0.73 on 95% of dekads, and lowest on dekads when the mean ETIa-WPR is highest.

The Koga has the lowest consistency of the schemes. Although the RMSE between L1 and L3 is lower, ranging from 0.3 to 0.7 mm/day, the median correlation is 0.67, and the median R^2 is 0.45.

Zankalon performed slightly better, with a median correlation of 0.71 and a median R^2 of 0.51. The RMSE is higher in Zankalon than the Koga, but this reflects the higher ETIa-WPR values found in the area. The ODN had the same RMSE (0.6 mm/day) as Zankalon and the highest range of RMSE (0.2–1.6 mm/day). The correlation and R^2 are also similar, with median values of 0.73 and 0.53, respectively. All schemes show similar per cent bias medians (9–12%). The only scheme that shows a systematic bias is ZAN, where the L1 is consistently higher ETIa-WPR values than L3.

The 10-daily average ETa-EC and ETIa-WPR for all three spatial resolutions at EG-ZAN are shown in Figure 10. The L1 and L2 ETIa-WPR show high consistency with each other. The L3 ETIa-WPR is consistently sitting between the ETa-EC and the L1 and L2 ETIa-WPR. All levels capture the overall ETa-EC seasonal trends. The L3 data shows a slightly lower R^2 (L3 = 0.66 and L1 = 0.69) and correlation (L3 = 0.53 and L1 = 0.68), but a much lower bias (L3 = 1.1 mm/day and L1 = 1.7 mm/day) and a lower RMSE (L3 = 1.0 mm/day and L1 = 2.2 mm/day) when compared with ETa-EC. The better R^2 and correlation reflect the L1 and L2 ETIa-WPR ability to capture the temporal fluctuations of ETa-EC better than L3 ETIa-WPR. An example of this is at dekad 1117, where L1 and L2 ETIa-WPR capture the ETa-EC dip, whereas L3 ETIa-WPR stays flat. The L3 ETIa-WPR have a better seasonal agreement with the ETa-lys for the summer maize crop in 2012 (L3 = 487 mm, L1 = 682 mm and ETa-lys = 543 mm).

The NDVI and ETIa-WPR for the 250 m buffer are shown in Figure 11 for the three spatial resolutions. The 30 m level is picking up more spatial variation (standard deviations: L3 = 0.05, L2 = 0.02; L1 = 0.02) at the site and has a lower mean NDVI for the site as compared to L2 and L1 (mean: L3 = 0.74; L2 = 0.82 and L1 = 0.83). This reflects the lower ETIa value for this dekad, which is more similar to the ETIa-EC (Figure 10) and shows some limitations in comparing L1 data to EC in a heterogeneous landscape.

4 | DISCUSSION

4.1 | Product accuracy

The ETIa-WPR results are comparable the improved MODIS global terrestrial ETa algorithm, MAPE of 24.6% as compared to EC measurement, when driven by the tower meteorological data (Mu et al., 2011). The ETIa-WPR error estimates, on average, are also close the average errors in EC measurements as EC measurements typically have errors of 20–30% (Allen et al., 2011; Blatchford,

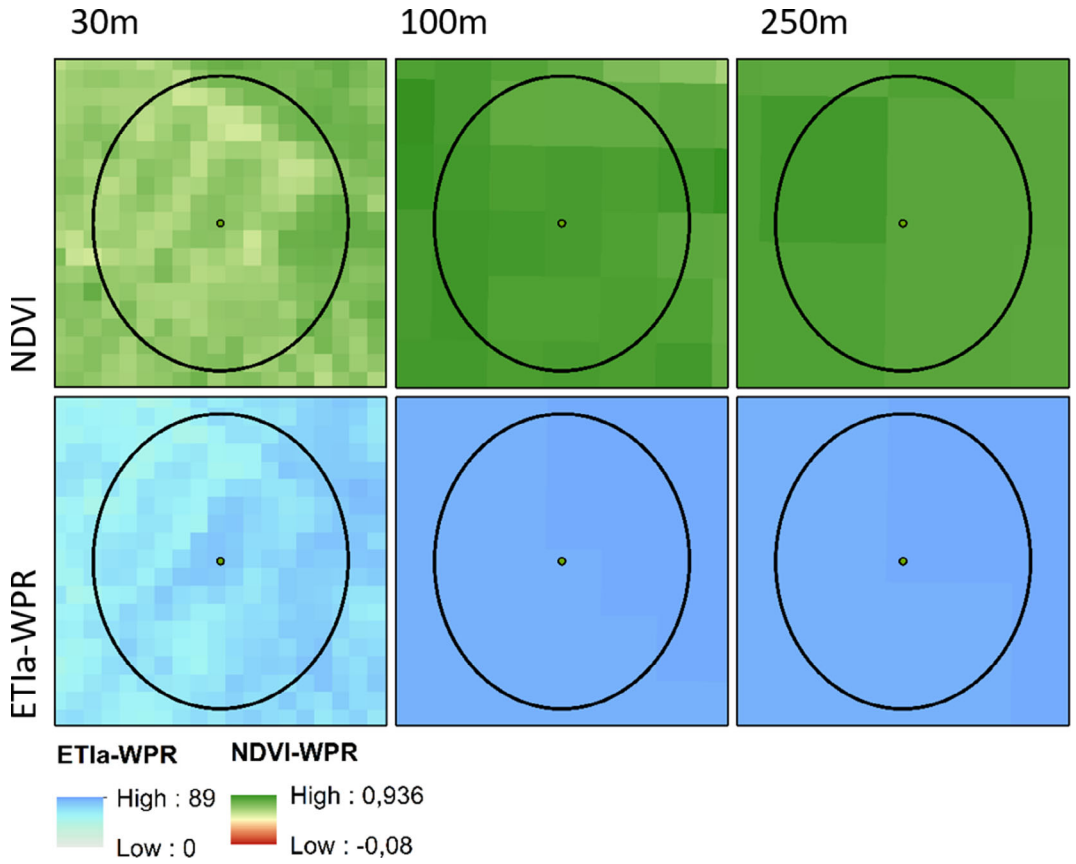

FIGURE 11 NDVI and ETIa-WPR for the EG-ZAN site for all three spatial resolutions (L3 = 30 m, L2 = 100 m and L1 = 250 m) on dekad 1222 (first dekad of August 2012). The point is the station location; the circle is the buffer used for data extraction to compare to the ETa-EC. NDVI, normalized difference vegetation index

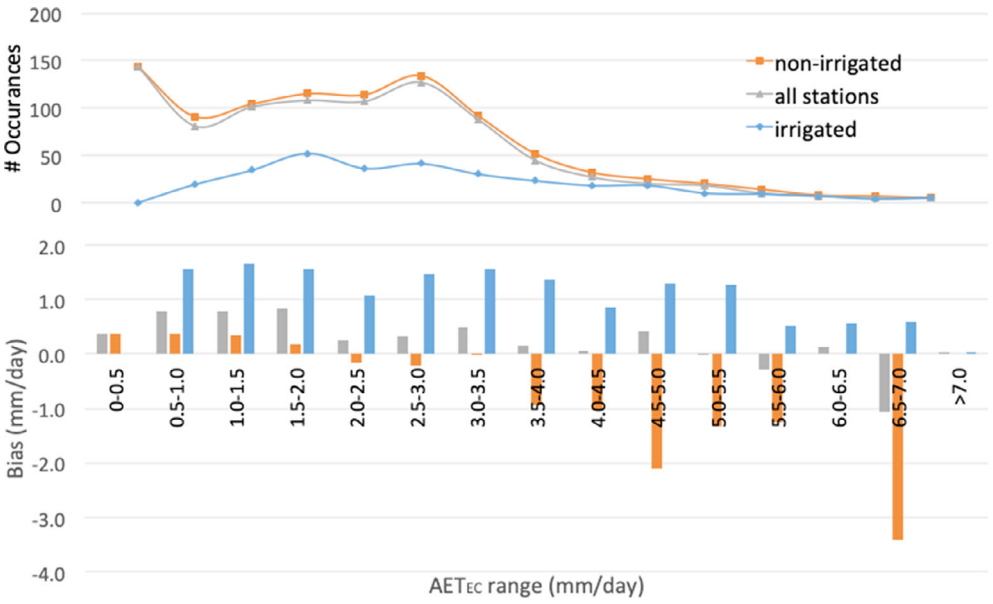

FIGURE 12 Upper—number of observations for a given ETa-EC range. Lower—bias of dekadal ETIa-WPR (mm/day), as compared to ETa-EC, plotted against the increasing ranges of ETa-EC (mm/day) for observations at natural vegetation sites (orange bar), irrigated agriculture sites (blue bar) and all sites (grey bar). Note that the ETa-EC in non-irrigated sites was only greater than 5.5 mm/day for three observations, they are not included in the bias calculations shown in the figure as it is not considered a representative sample size

Mannaerts, Zeng, Nouri, & Karimi, 2019), however, it appears that the ETIa-WPR is regularly overestimating ETIa, which is evident at local to basin level. Figure 12 shows the bias and number of observations between ETIa-WPR and ETa-EC for all EC observations disaggregated based on 0.5 mm/day ETa-EC increments. The results are further defined based on non-irrigated sites, irrigated agriculture and all stations. For non-irrigated sites, there is a positive bias (ETIa-WPR > ETa-EC) when the ETa-EC is less than 2.5 mm/day and becomes negative when the ETa-EC is greater than or equal to 2.5 mm/day (this reduced to 1.6 mm/day at a monthly scale). This bias increases, both positive and negative, as the ETa-EC deviates from 2.5 mm/day. The underestimation is further exacerbated by the fact that ETa-EC estimations can lead to underestimation of the latent energy or ETa-EC by 20% (Glenn et al., 2007; Wilson et al., 2002). Underestimation bias is larger than overestimation bias and increases with increasing ETIa-WPR. However, Africa as a continent is dry with long-term (2010–2015) average daily ETIa-WPR for the continent being 1.5 mm/day. Therefore, the ETIa-WPR frequently overestimates at the annual, basin scale. The irrigated sites (EG-SAA, EG-SAB and EG-ZAN) are overestimated for nearly all ETa-EC. The irrigated sites strongly influenced the overall bias, as these sites have many observation points. When irrigated and non-irrigated results are combined, the changing point where ETIa-WPR is greater than ETa-EC occurs when ETa-EC exceeds 3.5 mm/day.

4.1.1 | Why is WaPOR overestimating when ETIa is low?

ETIa-WPR is overestimating ETa in dry, hot, water-stressed conditions (e.g. water-limited). The ETIa-WPR estimates for prolonged dry weather and the dry seasons of WaPOR are usually higher than the observed values (flux towers, field). These overestimations are small in terms of absolute values (mm/day) but can lead to overestimation of results in higher annual ETIa-WPR when compared to water mass balance checks of river basins. The overestimation in dry regions is likely to be primarily due to the functioning of the SMC constraint or the too high SMC in dry regions.

The WaPOR SMC is considered, on average, high in arid regions (e.g. Figure 6) and therefore, ETIa-WPR is likely not effectively accounting for soil moisture limitations. The high SMC is resulting in an overestimation of the evaporation component in particular, as NDVI is low and therefore the region is dominated by the evaporation component of ETIa-WPR. Arid regions should be largely regulated by water availability rather than energy. Conversely, under well-water conditions, the Penman–Monteith method is primarily driven by Rn (e.g. energy limited) (Rana & Katerji, 1998). As Penman–Monteith is a linearized approximate solution, problems may occur in extreme conditions and errors in the soil evaporative term (Leca, Parisi, Lacointe, & Saudreau, 2011). Majozi et al. (2017b) noted that Penman–Monteith methods need to include a SMC constraint. Though the ETIa-WPR methodology does include a SMC constraint, overestimations in SMC are reducing its functionality. The SMC is estimated using the trapezoidal method (function of NDVI and LST). Where the NDVI is low, the LST component could be the primary contributing factor to SMC errors.

For water-stressed crops, crop resistance errors can attribute to the large error in ETa estimations, while for tall crops, the VPD can have a large influence on the error (Rana & Katerji, 1998). Extreme conditions include when aerodynamic resistance is high, >50 m/s (Paw, 1992). High aerodynamic resistance can occur in sparse vegetation, when surface temperature is much greater than air temperature (e.g. water-stressed conditions) and when wind speed is very low (Dhungel, Allen, Trezza, & Robison, 2014; Paw, 1992). Cleverly et al. (2013) and Steduto, Todorovic, Caliandro, and Rubino (2003) found when the standard aerodynamic resistance values were used the Penman–Monteith method over- and underestimated RET when RET is low and high respectively and suggested the aerodynamic

resistance should vary with climatic variables as it is responsive to relative humidity gradients.

It is recommended to further verify the behaviour of the SMC. The SMC relative moisture index is derived from LST and vegetation cover (NDVI) data. Therefore, verification against highest available physically based satellite soil moisture data (e.g. active microwave sensors on-board Sentinel-1A, Metop) is advised. It may be helpful to use SMC for transpiration and passive microwave sensors for evaporation.

The main source of error in the ET-WB method is the uncertainty in PCP. Studies on the CHIRPS PCP product shows high correlations, at monthly and regional scales, in Eastern Africa (r = 0.7–0.93) (Dinku et al., 2018; Gebrechorkos, Hülsmann, & Bernhofer, 2018) and Burkino Faso (r = 0.95) (Dembélé & Zwart, 2016) with little to no bias. Muthoni et al. (2019) reported that CHIRPS v2 slightly overestimated low-intensity rainfall below 100 mm and slightly underestimated high-intensity rainfall above 100 mm compared in Eastern and Southern Africa. On an annual, basin-scale, the CHIRPS PCP product does not show significant bias, except for in largely ungauged tropical basins (e.g. Congo) (Liu et al., 2016).

The Q component is less than 25% of the PCP in all but three basins used in the comparison, Central West Coast, West Coast and North East Coast (though in the North East Coast ETIa-WPR > PCP). In basins where Q is a significant component of the water balance, its uncertainty is going to have the largest influence on the uncertainty of the ETa-WB. The R^2 values of modelled GRDC Qmean against streamflow data were > 0.9 (Beck et al., 2015). Therefore, the Qmean is expected to be high in gauged basins. Unguaged basins, in the analysis, have higher uncertainty and introduce higher uncertainty into ETa-WB. Basins with no streamflow data include North Interior, North East Coast, Shebeli & Juba Basin and Limpopo. Of these basins only the North Interior has ETIa-WPR < PCP. If basins are removed from the analysis with missing streamflow data the regression between ETIa-WPR and ETa-WB only marginally improves (R^2 = 0.96 compared to R^2 = 0.94), suggesting the quality of Qmean is appropriate for the water balance check. Therefore, the large overestimations of ETIa-WPR should not be attributed to the simplified water balance approach.

Wetland and irrigated areas are expected to have ETIa greater than PCP. Wetland and irrigated areas represent 1% and < 2%, respectively of land cover in Africa and is suggested to have little impact on the overall water balance for most basins. The basins with the greatest irrigated land cover and the highest fraction of ETIa-WPR from irrigation, are Limpopo Basin (6.4% of land cover), Orange Basin (4.3% of land cover) and Indian Ocean Coast (6.7% of land cover). ETIa-WPR in these basins contribute to 6.0, 7.6 and 8.7% of the total evapotranspiration. For each of these basins, ETIa-WPR is greater than PCP by more than the fraction of ETIa-WPR from irrigation. Basins with large wetlands and high ground water availability include the Niger (Niger Delta), the Nile (the Nile Delta and Sudd wetland), the South Interior (Okavango Delta) (FAO and IHE Delft, 2019). However, large areas of shrubland and deciduous tree cover also have ETIa greater than PCP, when compared with the WaPOR land cover dataset (available on the WaPOR portal). The overestimation of ETIa compared to PCP on an annual basin appears to be more closely related to climate. Climate zones BSh, BWh, CWa and Aw have large areas with ETIa greater than or approximately equal to PCP at an annual scale. These zones are largely associated with basins with ETIa greater PCP.

4.1.2 | Why is WaPOR overestimating ETIa in irrigated fields?

ETIa-WPR is overestimating ETa dry, hot, non-water-stressed conditions (e.g. irrigated fields). These errors might lie in the FAO-Penman–Monteith method's and may be associated with local advection effects. Local advection may increase ETa over a water-limited field by up to 30% (De Bruin, Trigo, Bosveld, & Meirink, 2016; Trigo et al., 2018). There is an underlying assumption of no advection in the RET definition for a reference grass field (Allen et al., 1998). However, in small fields, under arid conditions with high temperatures, local advection effects may occur when warm, dry air formed over an upwind, adjacent field is advected horizontally over the well-watered fields (De Bruin & Trigo, 2019). This horizontal advection of sensible heat increases the ETa of water from well-watered areas, where SMC is high and not limiting, but will result in the overestimation of ETa in water-limited fields or areas. While the Egypt fields are well irrigated (Sugita et al., 2017) with SMC ranging from 0.6 to 1 throughout the irrigation season, surrounding fields are not, and frequently have low SMC or water limiting condition, which can potentially drive up the ETIa-WPR estimates. The Zankalon irrigated area, where EG-ZAN is located, has small fields, ~0.2 ha (Table 4), as does the EG-SAA and EG-SAB. Therefore, these sites may be particularly influenced by this effect as 0.2 ha is 3% of an L1—250 m pixel, 20% of an L2—100 m pixel and 200% of an L3—30 m pixel (e.g. see Figure 10).

4.1.3 | Why is WaPOR misrepresenting ETIa when ETIa is high in humid conditions?

ETIa-WPR is not representing ETa well in water unlimited conditions with high humidity. The Penman–Monteith method is not suitable for very low VPD (or high humidity) (Paw & Gao, 1988). Further, for tall crops, the VPD can have a considerable influence on the error (Rana & Katerji, 1998). It is not suitable in these conditions because of the linear assumption of saturated vapour pressure and air temperature. Paw (1992) advised that the use of non-linear equations should be used in extreme conditions to maintain errors of less than 10–15%.

Quality of input data is likely affecting the quality of the ETIa-WPR in these regions. Low-quality data or missing RH data means VPD is calculated from Tmin. In humid climates condensation occurs during the night, which leads to an overestimation of VPD (Allen et al., 1998), which is found when Penman–Monteith is applied

without RH data in humid regions of Ecuador (Córdova, Carrillo-Rojas, Crespo, Wilcox, & Célleri, 2015). In water unlimited regions, the overestimation of VPD can lead to higher ETa, as it is easier for the flux to occur when there is less moisture in the air. Further, these regions frequently contain low-quality NDVI and LST layers in these regions. This is resulting for example, in overestimation of radiation at GHANK skewing results at this location. The NDVI and LST quality layers are therefore a good indicator of the quality of the ETIa in these regions.

4.2 | Product consistency

There is very high consistency between L1 and L2 products. The high consistency is partly explained by the use of a downscaled MODIS product before the introduction of PROBA-V in 2014 and the SMC component, which is based on MODIS for both L1 and L2 for the entire database period. The high consistency suggests that at a given scale, for example basin scale, the 100 m product provides no additional value to the 250 m resolution. However, at higher resolution applications, the product does show spatial variation not captured by the L1 product (e.g. Figure 11) and may provide better insight into intra- and inter-field level variations.

The consistency between the L1 and L3 products is mixed. The Awash and ODN L3 areas show high consistency between L1 and L3. In the Koga, there is a strong positive bias for L1 ETIa-WPR, while the agreement between L1 and L3 in the Koga and in Zankalon is lower. These errors are likely largely attributed to the different input temporal and spatial resolutions available from the satellite platform combined with high spatial and temporal heterogeneity in the area (e.g. Koga and Zankalon have much smaller irrigated fields and higher crop diversity than the Awash and ODN–see Table 4). All levels have a dekadal timestep. However, the satellite revisit period varies, having revisits of 1-day, 2-days and 16 days for MODIS (L1), PROBA-V (L2) and Landsat (L3), respectively, with daily meteorological data input. The variation in the revisit period can lead to differences when interpolating images to a dekadal timescale, particularly in rainy periods and during the growing season (Gao, Masek, Schwaller, & Hall, 2006). Uncertainty of up to 40% has attributed to the difference in a 16-day revisit as compared to 4-day revisit, depending on climate and season (Guillevic et al., 2019), though this was without daily meteorological data as a tool for interpolation. Conversely, the L3 dataset can capture more spatial variability for a given image as compared to the L1 and L2 data, which is highly important when using non-linear models. Therefore, the L3 dataset is expected to perform better in areas of higher spatial heterogeneity (Sharma, Kilic, & Irmak, 2016).

5 | CONCLUSIONS

The WaPOR products for Africa and the Middle East provide the highest resolution continuous near real-time products available so far to monitor ETIa. Current validation efforts need to be continued and intensified to confirm the suitability of these products for various uses. However, significant issues with the sparseness of available ground-truth measurements make direct validation to in situ, insufficient as a sole means to validate the ETIa product over continental Africa. To compensate for insufficient ground-truth locations, we added physical consistency and level consistency checks as part of the validation analyses.

The ETIa-WPR product is responsive to general trends in the magnitude of ETIa for most climates and shows good correlations at both local (EC) and basin (WB) scales. In dry irrigated areas, WaPOR appears to be overestimating ETIa, particularly the coarse resolution. The overall ETIa-WPR MAPE of 26.3% on a monthly, point scale, 40.4% on a daily, point scale and 29.5% on an annual, basin scale. These are promising results considering that WaPOR presents a continental almost near real-time open-access dataset. Analysis of the intermediate data components provide insights into some of the possible causes of the over- and underestimation of ETI-WPR, which appear to be primarily driven by an overestimation of the SMC which is driving overestimation of evaporation. Users should also be cautious in applying the dataset in very hot, arid conditions, in high canopy (e.g. forests) and areas with large gaps in the NDVI- and LST quality layers. Further validation activities are suggested as new ground-data become available, particularly in cropped and irrigated areas.

ACKNOWLEDGEMENTS

We thank all of the authors in which we sourced data for validation. We would like to thank FAO who co-funded the operational methodology for an open-access database to monitor land and water productivity (WaPOR portal) and the FRAME consortium, in particular eLEAF and VITO as the primary producers of the WaPOR datasets. We gratefully acknowledge Dr Michaiki Sugita for providing the EG-ZAN, EG-SAA and EG-SAB EC data. We thank and acknowledge the efforts of researchers at the FluxNet, AMMA-CATCH and KWSTI flux tower sites for making their data available. We also thank the Global Runoff Data Centre (GRDC) and the U.S. Geological Survey (USGS) for making their observed Q data available and the NASA/EOS MODIS evapotranspiration team for the MOD16 global evapotranspiration product. We would also like to thank Dr Karin M. Viergever for being our key correspondence with the data provider. This work was funded by the United Nations Food and Agricultural Organization (FAO) as part of the Water Productivity Open-Access Portal (WaPOR) project, in which we undertook the validation efforts.

DATA AVAILABILITY STATEMENT

Data available on request from the authors, except for SMC and NDVI data layers which were provided by the FRAME consortium.

ORCID

Megan L. Blatchford https://orcid.org/0000-0002-1077-0709
Hamideh Nouri https://orcid.org/0000-0002-7424-5030

REFERENCES

Allen, R. G., Pereira, L. S., Howell, T. A., & Jensen, M. A. (2011). Evapotranspiration information reporting: I. Factors governing measurement accuracy. *Agricultural Water Management*, *98*, 899–920. https://doi.org/10.1016/j.agwat.2010.12.015

Allen, R. G., Pereira, L. S., Raes, D., & Smith, M. (1998). *FAO irrigation and drainage paper no. 56: Crop evapotranspiration*. Rome, Italy. Retrieved from: FAO—Food and Agriculture Organization of the United Nations. http://www.kimberly.uidaho.edu/water/fao56/fao56.pdf

Allen, R. G., Tasumi, M., & Trezza, R. (2007). Satellite-based energy balance for mapping evapotranspiration with internalized calibration (METRIC)—model. *Journal of Irrigation and Drainage Engineering*, *133* (4), 380–394. https://doi.org/10.1061/(ASCE)0733-9437(2007)133:4(380)

Ardö, J., Mölder, M., El-Tahir, B. A., & Elkhidir, H. A. M. (2008). Seasonal variation of carbon fluxes in a sparse savanna in semi arid Sudan. *Carbon Balance and Management*, *3*(7), 1–18. https://doi.org/10.1186/1750-0680-3-7

Atta, Y., Gaafar, I., Hassan, W., & El, A. (2015). Validation of accurate determination of maize water requirements in Nile Delta. In *International commission on irrigation and drainage. 26th Euro-Mediterranean regional conference and workshops, innovate to improve irrigation performances* (p. 4). Montpellier, France: International Commission on Irrigation and Drainage. Retrieved from. https://icid2015.sciencesconf.org/65471/document

Bastiaanssen, W. G. M., Cheema, M. J. M., Immerzeel, W. W., Miltenburg, I. J., & Pelgrum, H. (2012). Surface energy balance and actual evapotranspiration of the transboundary Indus Basin estimated from satellite measurements and the ETLook model. *Water Resources Research*, *48*, W11512. https://doi.org/10.1029/2011WR010482

Bastiaanssen, W. G. M., Menenti, M., Feddes, R., & Holtslag, A. A. (1998). A remote sensing surface energy balance algorithm for land (SEBAL). 1. Formulation. *Journal of Hydrology*, *212–213*(1998), 198–212. https://doi.org/10.1016/S0022-1694(98)00253-4

Beck, H. E., De Roo, A., & Van Dijk, A. I. J. M. (2015). Global maps of streamflow characteristics based on observations from several thousand catchments. *Journal of Hydrometeorology*, *16*, 1478–1501. https://doi.org/10.1175/JHM-D-14-0155.1

Blatchford, M. L., Mannaerts, C. M., Zeng, Y., Nouri, H., & Karimi, P. (2019). Status of accuracy in remotely sensed and in-situ agricultural water productivity estimates: A review. *Remote Sensing of Environment*, *234*, 111413. https://doi.org/10.1016/j.rse.2019.111413

Boulain, N., Cappelaere, B., Séguis, L., Favreau, G., & Gignoux, J. (2009). Water balance and vegetation change in the Sahel: A case study at the watershed scale with an eco-hydrological model. *Journal of Arid Environments*, *73*(12), 1125–1135. https://doi.org/10.1016/j.jaridenv.2009.05.008

Chishugi, J. B., & Alemaw, B. F. 2009. The hydrology of the Congo River Basin: A GIS-based hydrological water balance model. *World environmental and water resources congress 2009: Great rivers*. (pp. 1–16). Kansas City, MO: ASCE.

Chiti, T., Certini, G., Grieco, E., & Valentini, R. (2010). The role of soil in storing carbon in tropical rainforests: The case of Ankasa Park, Ghana. *Plant and Soil*, *331*(1–2), 453–461. https://doi.org/10.1007/s11104-009-0265-x

Cleverly, J., Chen, C., Boulain, N., Villalobos-Vega, R., Faux, R., Grant, N., … Eamus, D. (2013). Aerodynamic Resistance and Penman–Monteith evapotranspiration over a seasonally two-layered canopy in semiarid central Australia. *Journal of Hydrometeorology*, *14*(5), 1562–1570. https://doi.org/10.1175/jhm-d-13-080.1

Córdova, M., Carrillo-Rojas, G., Crespo, P., Wilcox, B., & Célleri, R. (2015). Evaluation of the Penman-Monteith (FAO 56 PM) method for calculating reference evapotranspiration using limited data. *Mountain Research and Development*, *35*(3), 230–239. https://doi.org/10.1659/mrd-journal-d-14-0024.1

De Bruin, H., Trigo, I., Bosveld, F., & Meirink, J. (2016). Thermodynamically based model for actual evapotranspiration of an extensive grass field close to FAO reference, suitable for remote sensing application. *Journal of Hydrometeorology*, *17*(5), 1373–1382. https://doi.org/10.1175/JHM-D-15-0006.1

De Bruin, H. A. R., & Trigo, I. F. (2019). A new method to estimate reference crop evapotranspiration from geostationary satellite imagery: Practical considerations. *Water*, *11*(2), 382. https://doi.org/10.3390/w11020382

Degefu, D. M., Weijun, H., Zaiyi, L., Liang, Y., Zhengwei, H., & Min, A. (2018). Mapping monthly water scarcity in global transboundary basins at country-basin mesh based spatial resolution. *Scientific Reports*, *8*(1), 1–10. https://doi.org/10.1038/s41598-018-20032-w

Dembélé, M., & Zwart, S. J. (2016). Evaluation and comparison of satellite-based rainfall products in Burkina Faso, West Africa. *International Journal of Remote Sensing*, *37*(17), 3995–4014. https://doi.org/10.1080/01431161.2016.1207258

Dhungel, R., Allen, R. G., Trezza, R., & Robison, C. W. (2014). Comparison of latent heat flux using aerodynamic methods and using the Penman-Monteith method with satellite-based surface energy balance. *Remote Sensing*, *6*(9), 8844–8877. https://doi.org/10.3390/rs6098844

Dinku, T., Funk, C., Peterson, P., Maidment, R., Tadesse, T., Gadain, H., & Ceccato, P. (2018). Validation of the CHIRPS satellite rainfall estimates over eastern Africa. *Quarterly Journal of the Royal Meteorological Society*, *144*, 292–312. https://doi.org/10.1002/qj.3244

FAO. (1997). *Irrigation potential in Africa: A basin approach*. Rome, Italy. Retrieved from: FAO. http://www.fao.org/3/W4347E/w4347e00.htm

FAO. (2020a). *WaPOR database methodology, V2 release (not yet published)*. Rome, Italy: Food and Agricultural Organization of the United Nations.

FAO. 2020b. *WaPOR—The FAO portal to monitor water productivity through open access or remotely sensed derived data*. FAO, Rome, Italy. Retrieved from https://wapor.apps.fao.org/home/1

FAO and IHE Delft. (2019). *WaPOR quality assessment technical report on the data quality of the WaPOR FAO database version 1.0* (134 pp). Rome, Italy: Food and Agricultural Organization of the United Nations. Retrieved from http://www.fao.org/3/ca4895en/ca4895en.pdf

Funk, C., Peterson, P., Landsfeld, M., Pedreros, D., Verdin, J., Shukla, S., … Michaelsen, J. (2015). The climate hazards infrared precipitation with stations—a new environmental record for monitoring extremes. *Scientific Data*, *2*, 150066. https://doi.org/10.1038/sdata.2015.66

Gao, F., Masek, J., Schwaller, M., & Hall, F. (2006). On the blending of the Landsat and MODIS surface reflectance: Predicting daily Landsat surface reflectance. *IEEE Transactions on Geoscience and Remote Sensing*, *44*(8), 2207–2218. https://doi.org/10.1109/TGRS.2006.872081

Gebrechorkos, S. H., Hülsmann, S., & Bernhofer, C. (2018). Evaluation of multiple climate data sources for managing environmental resources in East Africa. *Hydrology and Earth System Sciences*, *22*(8), 4547–4564. https://doi.org/10.5194/hess-22-4547-2018

Ghilain, N., Arboleda, A., & Gellens-Meulenberghs, F. (2011). Evapotranspiration modelling at large scale using near-real time MSG SEVIRI derived data. *Hydrology and Earth System Sciences*, *15*, 771–786. https://doi.org/10.5194/hess-15-771-2011

Glenn, E. P., Huete, A. R., Nagler, P. L., Hirschboeck, K. K., & Brown, P. (2007). Integrating remote sensing and ground methods to estimate evapotranspiration. *Critical Reviews in Plant Science*, *26*(3), 139–168. https://doi.org/10.1080/07352680701402503

Glenn, E. P., Huete, A. R., Nagler, P. L., & Nelson, S. G. (2008). Relationship between remotely-sensed vegetation indices, canopy attributes and plant physiological processes: What vegetation indices can and cannot tell us about the landscape. *Sensors*, *8*(4), 2136–2160. https://doi.org/10.3390/s8042136

Guillevic, P. C., Olioso, A., Hook, S. J., Fisher, J. B., Lagouarde, J. P., & Vermote, E. F. (2019). Impact of the revisit of thermal infrared remote sensing observations on evapotranspiration uncertainty—A sensitivity

study using AmeriFlux Data. *Remote Sensing*, *11*(5), 573. https://doi.org/10.3390/rs11050573

Hills, R. C. (1978). The structure of the inter-tropical convergence zone in equatorial Africa and its relationship to east African rainfall. *Transactions of the Institute of British Geographers*, *4*(3), 329–352. https://doi.org/10.2307/622055

Hobbins, M. T., Ramírez, J. A., & Brown, T. C. (2001). The complementary relationship in regional evapotranspiration: An enhanced advection-aridity model. *Water Resources Research*, *37*(5), 1389–1403. https://doi.org/10.1029/2000WR900359

Hu, G., Jia, L., & Menenti, M. (2015). Comparison of MOD16 and LSA-SAF MSG evapotranspiration products over Europe for 2011. *Remote Sensing of Environment*, *156*, 510–526. https://doi.org/10.1016/j.rse.2014.10.017

Kottek, M., Grieser, J., Beck, C., Rudolf, B., & Rubel, F. (2006). World map of the Köppen–Geiger climate classification updated. *Meteorologische Zeitschrift*, *15*(3), 259–263. https://doi.org/10.1127/0941-2948/2006/0130

LBPTC. (2010). *Joint Limpopo River Basin study scoping phase final report*. Federal Ministry for Economic Cooperation and Development and DFID. Retrieved from http://www.limpopo.riverawarenesskit.org/LIMPOPORAK_COM/_SYSTEM/DMSSTORAGE/3451EN/LIMCOM2010_SCOPINGSTUDY_ENG.PDF

Leca, A., Parisi, L., Lacointe, A., & Saudreau, M. (2011). Comparison of Penman–Monteith and non-linear energy balance approaches forestimating leaf wetness duration and apple scab infection. *Agricultural and Forest Meteorology*, *151*, 1158–1162. https://doi.org/10.1016/j.agrformet.2011.04.010

Lehner, B., & Grill, G. (2013). Global river hydrography and network routing: Baseline data and new approaches to study the world's large river systems. *Hydrological Processes*, *27*(15), 2171–2186. https://doi.org/10.1002/hyp.9740

Li, K. Y., Coe, M. T., & Ramankutty, N. (2005). Investigation of hydrological variability in West Africa using land surface models. *Journal of Climate*, *18*(16), 3173–3188. https://doi.org/10.1175/JCLI3452.1

Liu, W., Wang, L., Zhou, J., Li, Y., Sun, F., Fu, G., & Li, X. (2016). A worldwide evaluation of basin-scale evapotranspiration estimates against the water balance method. *Journal of Hydrology*, *238*, 82–95. https://doi.org/10.1016/j.jhydrol.2016.04.006

Majozi, N. P., Mannaerts, C. M., Ramoelo, A., Mathieu, R., Mudau, A. E., & Verhoef, W. (2017a). An intercomparison of satellite-based daily evapotranspiration estimates under different eco-climatic regions in South Africa. *Remote Sensing*, *9*(4), 307. https://doi.org/10.3390/rs9040307

Majozi, N. P., Mannaerts, C. M., Ramoelo, A., Mathieu, R., Nickless, A., & Verhoef, W. (2017b). Analysing surface energy balance closure and partitioning over a semi-arid savanna FLUXNET site in Skukuza, Kruger National Park, South Africa. *Hydrology and Earth System Sciences*, *21*(7), 3401–3415. https://doi.org/10.5194/hess-21-3401-2017

Mamadou, O., Cohard, J. M., Galle, S., Awanou, C. N., Diedhiou, A., Kounouhewa, B., & Peugeot, C. (2014). Energy fluxes and surface characteristics over a cultivated area in Benin: Daily and seasonal dynamics. *Hydrology and Earth System Sciences*, *18*, 893–914. https://doi.org/10.5194/hess-18-893-2014

Matondo, J. I., & Mortensen, P. (1998). Water resource assessment for the Zambezi River Basin. *Water International*, *23*(4), 256–262. https://doi.org/10.1080/02508069808686780

McDonald, J. E. (1961). On the ratio of evaporation to precipitation. *Bulletin of the American Meteorological Society*, *42*(3), 185–189. https://doi.org/10.1175/1520-0477-42.3.185

Merbold, L., Ardö, J., Arneth, A., Scholes, R. J., Nouvellon, Y., Grandcourt, A., … Kergo, W. L. (2009). Precipitation as driver of carbon fluxes in 11 African ecosystems. *Biogeosciences*, *6*(6), 1027–1041. https://doi.org/10.5194/bg-6-1027-2009

Miralles, D. G., Holmes, T. R. H., De Jeu, R. A. M., Gash, J. H., Meesters, A. G. C. A., & Dolman, A. J. (2011). Global land-surface evaporation estimated from satellite-based observations. *Hydrology and Earth System Sciences*, *15*, 453–469. https://doi.org/10.5194/hess-15-453-2011

Morisette, J. T., Privette, J. L., & Justice, C. O. (2002). A framework for the validation of MODIS Land products. *Remote Sensing of Environment*, *83*(1–2), 77–96. https://doi.org/10.1016/S0034-4257(02)00088-3

Morisette, J. T., Privette, J. L., Justice C. O., & Running S. W. (1998, September). *MODIS land validation plan*. Retrieved from https://modis.gsfc.nasa.gov/data/atbd/land_val.pdf

Mu, Q., Heinsch, F. A., Zhao, M., & Running, S. W. (2007). Development of a global evapotranspiration algorithm based on MODIS and global meteorology data. *Remote Sensing of Environment*, *106*(3), 285–304. https://doi.org/10.1016/j.rse.2007.04.015

Mu, Q., Zhao, M., & Running, S. W. (2011). Improvements to a MODIS global terrestrial evapotranspiration algorithm. *Remote Sensing of Environment*, *115*(8), 1781–1800. https://doi.org/10.1016/j.rse.2011.02.019

Mu, Q., Zhao, M., & Running, S. W. (2013). *Algorithm theoretical basis document: MODIS global terrestrial evapotranspiration (ET) product (NASA MOD16A2/A3) collection 5*. NASA Headquarters. Retrieved from https://modis-land.gsfc.nasa.gov/pdf/MOD16ATBD.pdf

Mueller, B., Seneviratne, S. I., Jimenez, C., Corti, T., Hirschi, M., Balsamo, G., … Kergo, W. L. (2011). Evaluation of global observations-based evapotranspiration datasets and IPCC AR4 simulations. *Geophysical Research Letters*, *38*(6), 1–7. https://doi.org/10.1029/2010GL046230

Muthoni, F. K., Odongo, V. O., Ochieng, J., Mugalavai, E. M., Mourice, S. K., Hoesche-Zeledon, I., … Bekunda, M. (2019). Long-term spatial-temporal trends and variability of rainfall over Eastern and Southern Africa. *Theoretical and Applied Climatology*, *137*, 1869–1882. https://doi.org/10.1007/s00704-018-2712-1

Nagler, P. L., Glenn, E. P., Nguyen, U., Scott, R. L., & Doody, T. (2013). Estimating riparian and agricultural actual evapotranspiration by reference evapotranspiration and MODIS enhanced vegetation index. *Remote Sensing*, *5*(8), 3849–3871. https://doi.org/10.3390/rs5083849

Nouri, H., Glenn, E. P., Beecham, S., Boroujeni, S. C., Sutton, P., Alaghmand, S., … Nagler, P. (2016). Comparing three approaches of evapotranspiration estimation in mixed urban vegetation: Field-based, remote sensing-based and observational-based methods. *Remote Sensing*, *8*(6), 492. https://doi.org/10.3390/rs8060492

Odongo, V. O., Van der Tol, C., Becht, R., Hoedjes, J. C. B., Ghimire, C. P., & Su, Z. (2016). Energy partitioning and its controls over a heterogeneous semi-arid shrubland ecosystem in the Lake Naivasha Basin, Kenya. *Ecohydrology*, *9*(7), 1358–1375. https://doi.org/10.1002/eco.1732

Paw, K. T. (1992). A discussion of the Penman form equations and comparisons of some equations to estimate latent energy flux density. *Agricultural and Forest Meteorology*, *57*(4), 297–304. https://doi.org/10.1016/0168-1923(92)90125-N

Paw, U. K. T., & Gao, W. (1988). Applications of solutions to non-linear energy budget equations. *Agricultural and Forest Meteorology*, *43*, 121–145. https://doi.org/10.1016/0168-1923(88)90087-1

Ramier, D., Boulain, N., Cappelaere, B., Timouk, F., Rabanit, M., Lloyd, C. R., … Wawrzyniak, V. (2009). Towards an understanding of coupled physical and biological processes in the cultivated Sahel – 1. Energy and water. *Journal of Hydrology*, *375*(1–2), 204–216. https://doi.org/10.1016/j.jhydrol.2008.12.002

Rana, G., & Katerji, N. (1998). A measurement based sensitivity analysis of the Penman-Monteith actual evapotranspiration model for crops of different height and in contrasting water status. *Theoretical and Applied Climatology*, *60*, 141–149. https://doi.org/10.1007/s007040050039

Rienecker, M. M., Suarez, M. J., Gelaro, R., Todling, R., Bacmeister, J., Liu, E., … Woollen, J. (2011). MERRA: NASA's modern-era retrospective analysis for research and applications. *Journal of Climate*, *24*, 3624–3648. https://doi.org/10.1175/JCLI-D-11-00015.1

Rockström, J., Falkenmark, M., Lannerstad, M., & Karlberg, L. (2012). The planetary water drama: Dual task of feeding humanity and curbing climate change. *Geophysical Research Letters*, *39*(15), 1–8. https://doi.org/10.1029/2012GL051688

Schneider, P., Ghent, D., Prata, F., Corlett, G. K., & Remedios, J. J. (2012). *AATSR validation: LST validation protocol*. ESA contract number: 19054/05/NL/FF. Retrieved from http://lst.nilu.no/Portals/73/Docs/Reports/UL-NILU-ESA-LST-LVP-Issue1-Rev0-1604212.pdf

Sebhat, M. Y., & Wenninger, J. (2014). Water balance of the Juba and Shabelle Rivers basins the Horn of Africa. *International Journal of Agricultural Policy and Research*, *2*(6), 238–255. https://doi.org/10.14303/irjas.2014.027

Senay, G. B., Budde, M., & Verdin, J. P. (2011). Enhancing the simplified surface energy balance (SSEB) approach for estimating landscape ET: Validation with the METRIC model. *Agricultural Water Management*, *98*, 606–618. https://doi.org/10.1016/j.agwat.2010.10.014

Sharma, V., Kilic, A., & Irmak, S. (2016). Impact of scale/resolution on evapotranspiration from Landsat and MODIS images. *Water Resources Research*, *52*(3), 1800–1819. https://doi.org/10.1002/2015WR017772

Sjöström, M., Zhao, M., Archibald, S., Arneth, A., Cappelaere, B., & Ardö, J. (2013). Evaluation of MODIS gross primary productivity for Africa using eddy covariance data. *Remote Sensing of Environment*, *131*, 275–286. https://doi.org/10.1016/j.rse.2012.12.023.

Steduto, P., Todorovic, M., Caliandro, A., & Rubino, P. (2003). Daily reference evapotranspiration estimates by the Penman-Monteith equation in Southern Italy. Constant vs. variable canopy resistance. *Theoretical and Applied Climatology*, *74*(3–4), 217–225. https://doi.org/10.1007/s00704-002-0720-6

Su, Z. (2002). The surface energy balance system (SEBS) for estimation of turbulent heat fluxes. *Hydrology and Earth System Sciences Discussions*, *6*(1), 85–100. https://doi.org/10.5194/hess-6-85-2002

Sugita, M., Matsuno, A., El-Kilani, R. M. M., Abdel-Fattah, A., & Mahmoud, M. A. (2017). Crop evapotranspiration in the Nile Delta under different irrigation methods. *Hydrological Sciences Journal*, *62*(10), 1618–1635. https://doi.org/10.1080/02626667.2017.1341631

Swinnen, E., Van Hoolst, R., & Toté, C. (2015). *Gio global land component—Lot I "Operation of the global land component"*. Framework service contract N° 388533 (JRC). Quality assessment report. Dry matter productivity (DMP)—PROBA-V, Algorithm theoretical basis document, Issue I1.01. VITO, EC Copernicus Global Land, Brussels. Retrieved from https://land.copernicus.eu/global/sites/cgls.vito.be/files/products/GIOGL1_QAR_DMP300m_V1_I1.12.pdf

Tagesson, T., Fensholt, R., Guiro, I., Rasmussen, M. O., Huber, S., Mbow, C., … Ardö, J. (2015). Ecosystem properties of semiarid savanna grassland in West Africa and its relationship with environmental variability. *Global Change Biology*, *21*(1), 250–264. https://doi.org/10.1111/gcb.12734

The Nile Basin Initiative Secretariat. (2014). Nile waters technical bulletin from the Nile Basin Initiative Secretariat, understanding Nile Basin hydrology mapping actual evapotranspiration over the Nile Basin. Entebbe, Ethiopia. Retrieved from www.nilebasin.org

Trigo, I. F., De Bruin, H., Beyrich, F., Bosveld, F. C., Gavilán, P., Groh, J., & López-Urrea, R. (2018). Validation of reference evapotranspiration from Meteosat Second Generation (MSG) observations. *Agricultural and Forest Meteorology*, *259*, 271–285. https://doi.org/10.1016/j.agrformet.2018.05.008

USAID. (2016, May 6). *Southern Africa—Drought fact sheet #4, Fiscal year (FY) 2016* (pp. 1–9). Retrieved from https://www.usaid.gov/sites/default/files/documents/1866/southern_africa_dr_fs02_05-06-2016.pdf

Velpuri, N. M., Senay, G. B., Singh, R. K., Bohms, S., & Verdin, J. P. (2013). A comprehensive evaluation of two MODIS evapotranspiration products over the conterminous United States: Using point and gridded FLUXNET and water balance ET. *Remote Sensing of Environment*, *139*, 35–39. https://doi.org/10.1016/j.rse.2013.07.013

Voisin, N., Wood, A. W., & Lettenmaier, D. P. (2008). Evaluation of precipitation products for global hydrological prediction. *Journal of Hydrometeorology*, *9*, 388–407. https://doi.org/10.1175/2007JHM938.1

Wang, D., & Alimohammadi, N. (2012). Responses of annual runoff, evaporation, and storage change to climate variability at the watershed scale. *Water Resources Research*, *48*, W05546. https://doi.org/10.1029/2011WR011444

Wilson, K., Goldstein, A., Falge, E., Aubinet, M., Baldocchi, D. D., Berbigier, P., … Verma, S. (2002). Energy balance closure at FLUXNET sites. *Agricultural and Forest Meteorology*, *113*(1–4), 223–243. https://doi.org/10.1016/S0168-1923(02)00109-0

Zeng, Y., Su, Z., Barmpadimos, I., Perrels, A., Poli, P., Boersma, K. F., … Timmermans, W. (2019). Towards a traceable climate service: Assessment of quality and usability of essential climate variables. *Remote Sensing*, *11*(10), 1186. https://doi.org/10.3390/rs11101186

Zeng, Y., Su, Z., Calvet, J. C., Manninen, T., Swinnen, E., Schulz, J., … Meurey, C. (2015). Analysis of current validation practices in Europe for space-based climate data records of essential climate variables. *International Journal of Applied Earth Observation and Geoinformation*, *42*, 150–161. https://doi.org/10.1016/j.jag.2015.06.006

Zhang, Y., Leuning, R., Chiew, F. H. S., Wang, E., Zhang, L., Liu, C., … Jung, M. (2012). Decadal trends in evaporation from global energy and water balances. *Journal of Hydrometeorology*, *13*(1), 379–391. https://doi.org/10.1175/JHM-D-11-012.1

How to cite this article: Blatchford ML, Mannaerts CM, Njuki SM, et al. Evaluation of WaPOR V2 evapotranspiration products across Africa. *Hydrological Processes*. 2020;1–22. https://doi.org/10.1002/hyp.13791